CHAPTER IV

RESULTS AND DISCUSSION

4.1 The physical properties of SBA-15

4.1.1 XRD patterns of SBA-15

The small-angle XRD patterns of the as-synthesized and calcined SBA-15 depicted in Figure 4.1. The assignment of those peaks were known as (100), (110) and (200) reflection planes, which were the characteristic pattern of hexagonal mesoporous structures [14]. Peak positions were located at quite low 2 theta values due to the lack of short-range order of its structure. After calcined in air at 550°C for 5 h, the XRD pattern showed that the hexagonal structure was remained and peak intensity at (100) reflection increases which resulting from the removal of triblock copolymer template from the pores of materials. Notice that the XRD pattern of the calcined sample was slightly shifted to the larger angle because the unit cell contracted after heated at high temperature (550°C) [73].

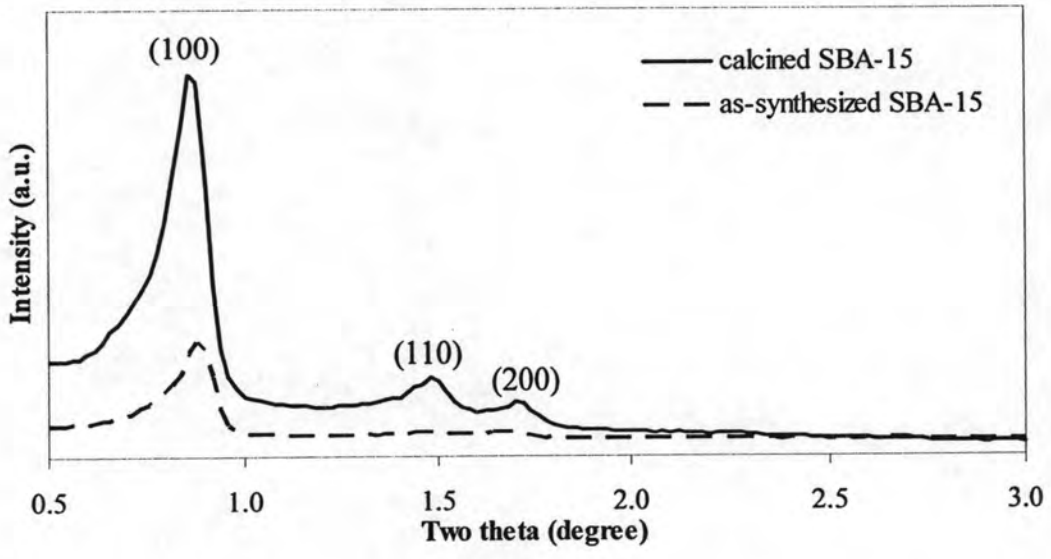

Figure 4.1 XRD patterns of as-synthesized SBA-15 and calcined SBA-15.

4.1.2 Sorption properties of SBA-15

The adsorption isotherm and pore size distribution of calcined SBA-15 showed in Figure 4.2. It exhibited a type IV adsorption isotherm which was a characteristic pattern of mesoporous materials. Considering the pore size distribution of resulted sample in Figure 4.2(b), narrow pore size distribution was found in SBA-15 at the pore diameter of 9.23 nm. The multipoint Brunauer, Emmett and Teller (BET) method was used in measuring total surface area of SBA-15, which was 925 m^2/g.

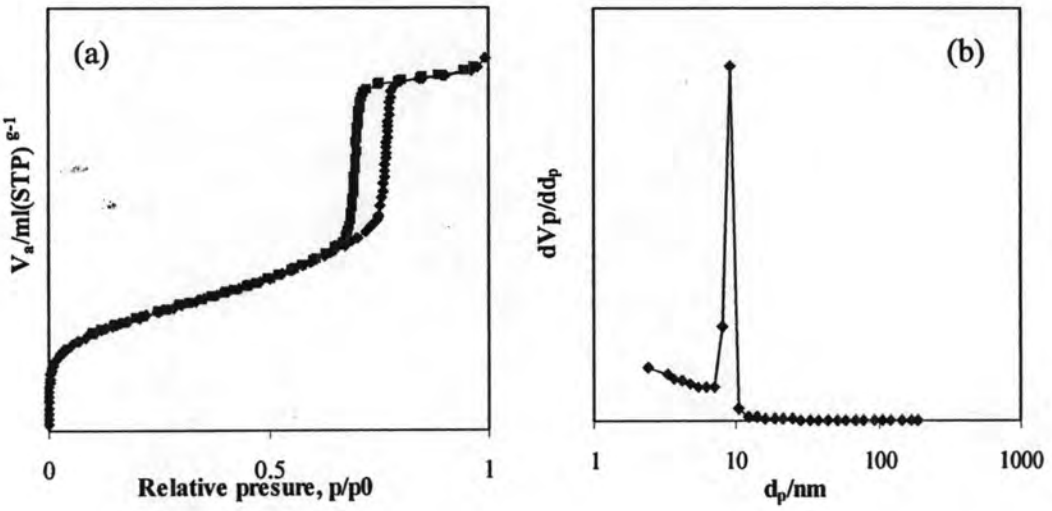

Figure 4.2 (a) N_2 adsorption-desorption isotherm and (b) BJH-pore size distribution of calcined SBA-15.

4.1.3 SEM images of SBA-15

The SEM images of calcined SBA-15 sample showed in Figure 4.3. All calcined samples were aggregated particles with rope-liked structure. The average size of particle was 0.8×1.1 μm.

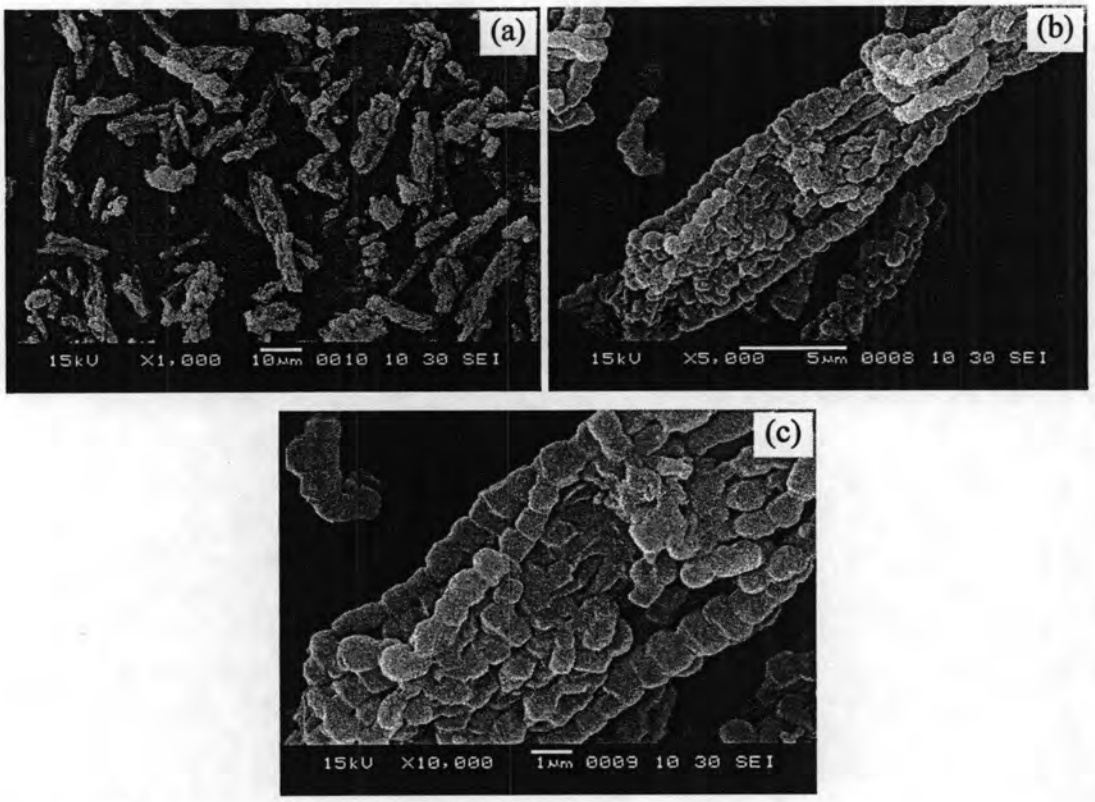

Figure 4.3 SEM images of calcined SBA-15 at different magnifications (a) ×500, (b) ×5,000, and (c) ×10,000.

4.1.4 TEM image of SBA-15

The microstructure of SBA-15 powder was examined by TEM micrograph as shown in Figure 4.4. The TEM image presented the well-ordered hexagonal arrays of one-dimensional mesoporous channels of SBA-15.

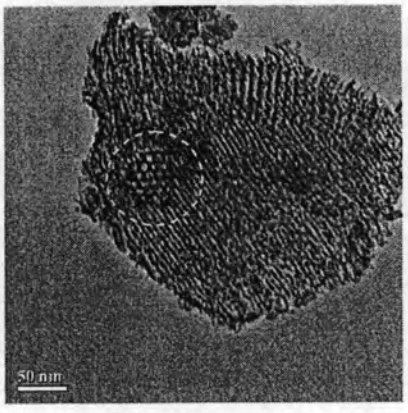

Figure 4.4 TEM image of calcined SBA-15.

4.2 The physical-chemical properties of Al-SBA-15

4.2.1 XRD patterns of Al-SBA-15

The sample of Al-SBA-15 was synthesized with Si/Al ratio in gel about 10 by alumination method following Kevan *et al.* [72]. After alumination, the XRD pattern showed clearly hexagonal plane which implied to the thermal stability of SBA-15 structure. The XRD pattern of Al-SBA-15 compared to calcined SBA-15 showed in Figure 4.5. The intensity of the (100) reflection increases when Al was added in SBA-15 structure. In addition (100) reflection was shifted slightly to higher angle comparing to SBA-15 resulting from the shrinkage during the recalcination process or change in lattice parameters and d-spacing due to Al inclusion in crystal structure of SBA-15 [48].

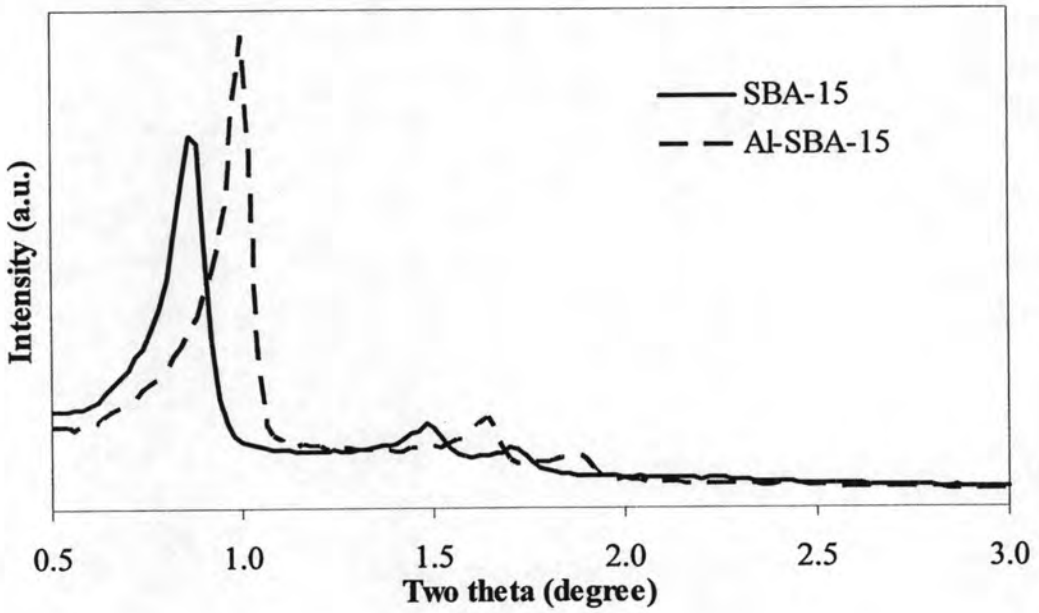

Figure 4.5 XRD patterns of calcined SBA-15 and Al-SBA-15.

4.2.2 Sorption properties of Al-SBA-15

Nitrogen adsorption-desorption isotherm of the post synthesized Al-SBA-15 showed in Figure 4.6. The sample performed hysteresis loop of type IV adsorption isotherm, typical for a mesoporous material. The BET was found specific surface area of

Al-SBA-15 450 m^2/g which lower than pure SBA-15 and BJH plot in Figure 4.6(b) showed narrow pore size distribution of Al-SBA-15 at the pore diameter 9.23 nm. Considering the effect of aluminum in catalyst, wall thickness was calculated in the same method as Stucky *et al.* [14]. The results of d-spacing of the (100) reflection plane of SBA-15 and Al-SBA-15 were 9.69 and 9.04 nm, respectively. After calculation the value of the wall thickness of SBA-15 and Al-SBA-15 were 1.96 and 1.21 nm, respectively.

The value of wall thickness was calculated based on the equations as follows:

$$\text{Wall thickness} = a_0\text{-pore size} \quad (1)$$

$$a_0 = 2\times d_{(100)}/\sqrt{3} \quad (2)$$

a_0 = total specific surface area from BET method

$d_{(100)}$ = d-spacing of the (100) reflection plane from XRD method

The data showed the wall thickness decrease when aluminum atoms were incorporated in SBA-15 structure, corresponding to the decrease in d-spacing as $d_{(100)}$ in the equation (2).

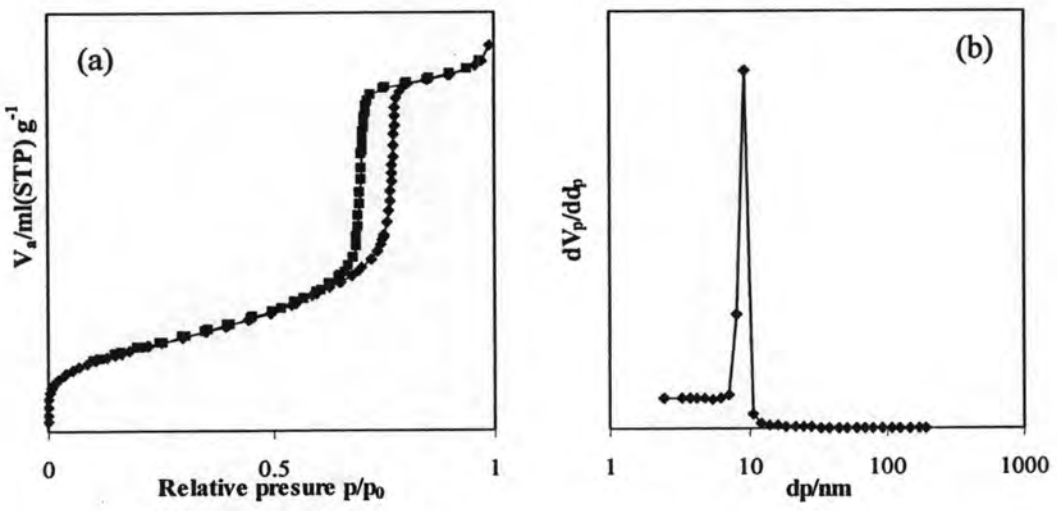

Figure 4.6 (a) N_2 adsorption-desorption isotherm and (b) BJH-pore size distribution of calcined Al-SBA-15.

4.2.3 Elemental analysis of Al-SBA-15

The Si/Al ratio in gel calculated from gel composition and in Al-SBA-15 product calculated by ICP-AES technique were 10.00 and 7.79, respectively. The elemental analysis result proved that aluminum elements were in the solid structure of SBA-15. The Si/Al molar ratio in the gel of Al-SBA-15 in preparation step was higher than found in synthetic matter. That may be caused by the structural framework of pure silica SBA-15 was collapsed, thus the silica in the framework was substituted by aluminum.

However, data from only ICP-AES technique could not exhibit the position of aluminum atom, whether it located in framework or extra-framework, therefore data from ^{27}Al-NMR was identified.

4.2.4 ^{27}Al-MAS-NMR spectrum of Al-SBA-15

Solid state ^{27}Al-MAS-NMR could identify the form of aluminum atoms that were located in tetrahedral form (at the framework) or found in octahedral form (non-framework). The ^{27}Al-MAS-NMR spectrum of Al-SBA-15 catalyst presented in Figure 4.7.

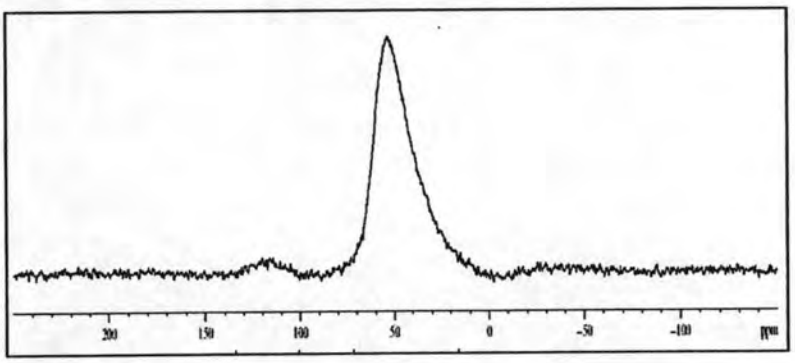

Figure 4.7 ^{27}Al-MAS-NMR spectrum of calcined Al-SBA-15.

From ^{27}Al-MAS-NMR spectrum, Al-SBA-15 sample exhibited only one intense signal of the framework site at 50 ppm indicating the Al atoms were incorporated into the SBA-15 at purely tetrahedral framework position. In contrast to other reports [73-75] that ^{27}Al-MAS-NMR spectrum of Al-SBA-15 samples exhibited extra-framework at position of octahedral coordination at 20 ppm.

4.2.5 SEM images of Al-SBA-15

The SEM images of Al-SBA-15 sample showed small rod particles (Figure 4.8). After aluminum addition, some small rod particles were separated from the rope-liked agglomeration of SBA-15. Al-SBA-15 performed many rod particles that were broken from SBA-15 showed in Figure 4.3. However the rod shape of individual particle remained the same as pure silica matter.

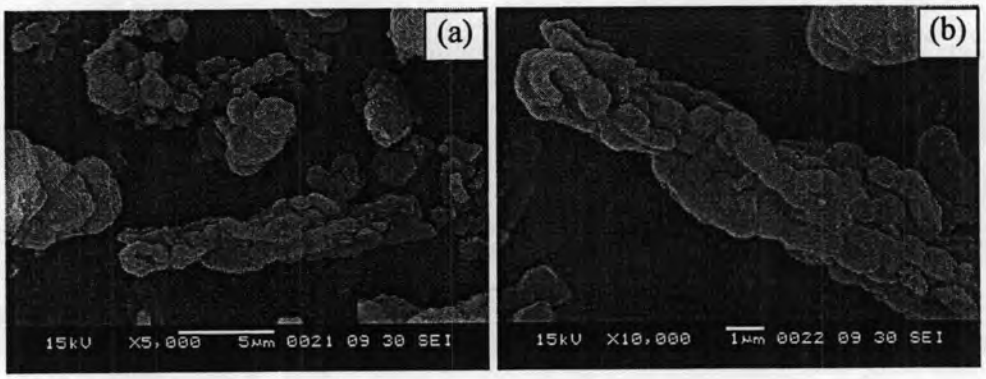

Figure 4.8 SEM images of calcined Al-SBA-15 at different magnifications (a) ×5,000 and (b) ×10,000.

4.2.6 TEM images of Al-SBA-15

The micrograph of SBA-15 powder was examined by TEM showed in Figure 4.9. The TEM image exhibited the well-ordered hexagonal array of one-dimensional mesoporous channels of Al-SBA-15. The introduction of Al into porous material framework was leaded to the formation of Al in tetrahedral site which expresses the acidity of Al-SBA-15 structure. Hence, TEM image was confirmed no presented metallic Al particle.

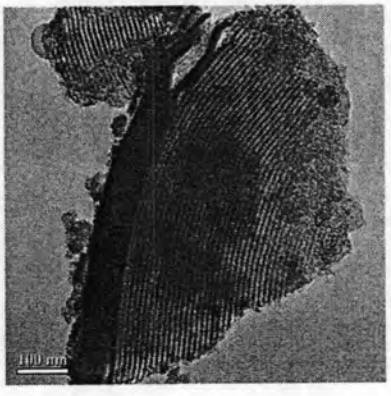

Figure 4.9 TEM image of Al-SBA-15.

4.3 The physical properties of M-SBA-15 (M = Ni, Pt, Pd and Ru)

4.3.1 XRD patterns of M-SBA-15 (M = Ni, Pt, Pd and Ru)

The XRD patterns of M-SBA-15 samples prepared by wet impregnation method compared with SBA-15 showed in Figure 4.10. For all M-SBA-15 products, similar three well-resolved peaks were observed. From XRD patterns, all of metals increased the intensity of the (100) reflection. The prominent XRD reflection (100) slightly shifted towards a higher angle was observed for the metal impregnation SBA-15 comparing to SBA-15, also similar to that detected from Al-SBA-15 resulting from the shrinkage during the recalcination process because the unit cell contracted after heated at high temperature.

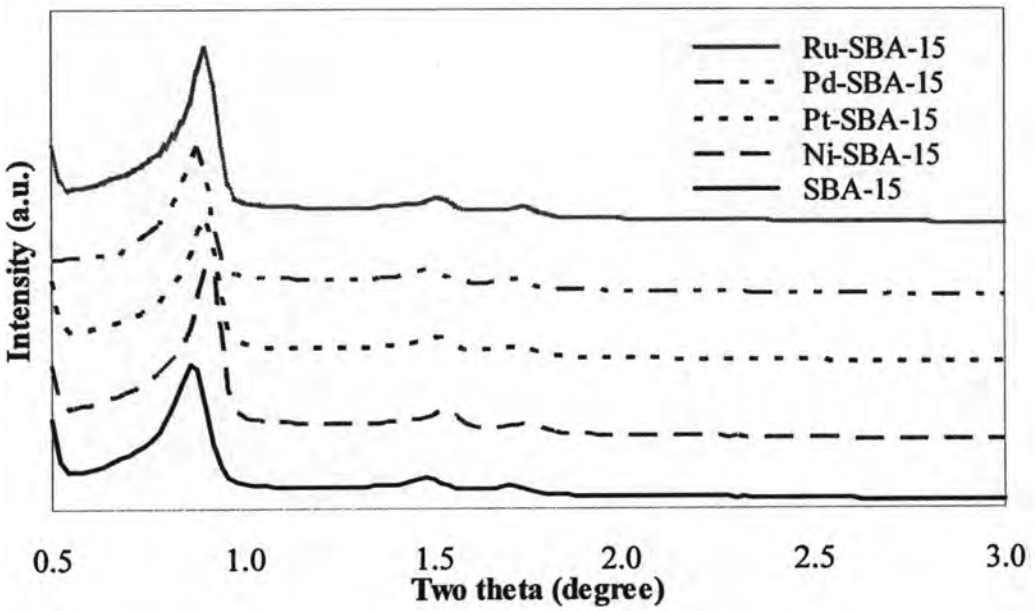

Figure 4.10 XRD patterns of calcined SBA-15 and M-SBA-15.

4.3.2 Sorption properties of M-SBA-15 (M = Ni, Pt, Pd and Ru)

The N_2 adsorption-desorption isotherms of the calcined M-SBA-15 catalysts showed in Figure 4.11. All samples exhibited type IV isotherm which was typical for mesoporous material. Furthermore, the shape of the adsorption-desorption isotherm of M-SBA-15 were similar to that of SBA-15. These results indicate that

uniform pore structure of SBA-15 was maintained even after impregnation. Textural properties of calcined catalysts were shown in Table 4.1.

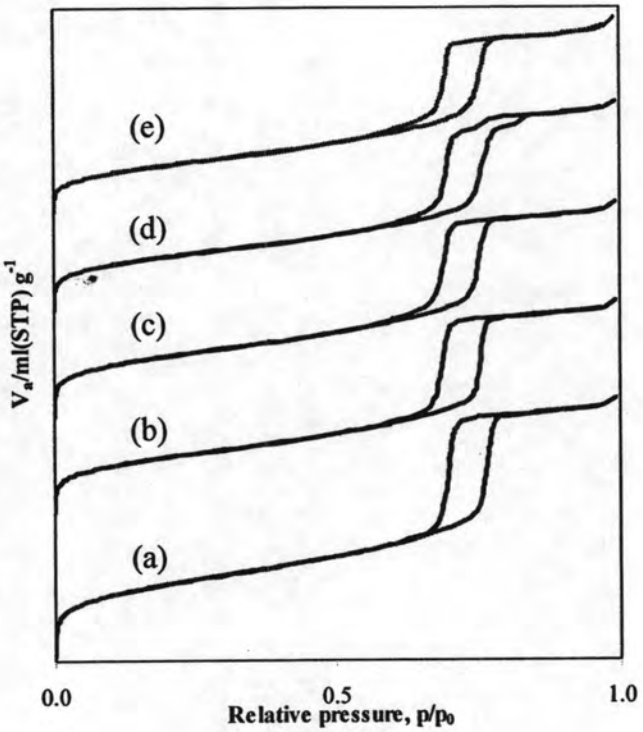

Figure 4.11 N_2 adsorption-desorption isotherms of (a) SBA-15, (b) Ni-SBA-15, (c) Pt-SBA-15, (d) Pd-SBA-15 and (e) Ru-SBA-15.

Table 4.1 Textural properties of calcined SBA-15 and M-SBA-15

Sample	Total specific surface area[a] ($m^2 \cdot g^{-1}$)	Pore size distribution[b] (nm)	Mesopore volume[b] ($cm^3 \cdot g^{-1}$)	$d_{(100)}$[c] (nm)	Wall thickness[d] (nm)
SBA-15	925	9.23	1.239	9.69	1.96
Ni-SBA-15	728	9.23	1.032	10.05	2.37
Pt-SBA-15	849	9.23	1.189	10.04	2.36
Pd-SBA-15	740	9.23	1.045	10.10	2.43
Ru-SBA-15	673	9.23	0.815	10.06	2.39

[a]Calculated using the BET plot method,
[b]Calculated using the BJH method,
[c]Calculated using XRD, Jade5.6,
[d]Calculated as: a_0-pore size ($a_0 = 2 \times d_{(100)} / \sqrt{3}$)

Pore size distributions of M-SBA-15 were shown in Figure 4.12. All samples performed a narrow distribution with the pore size of 9.23 nm. By comparing to the pore size distribution of pure silica SBA-15, the pore size of all M-SBA-15 samples still remained unchange, indicating the stability of M-SBA-15.

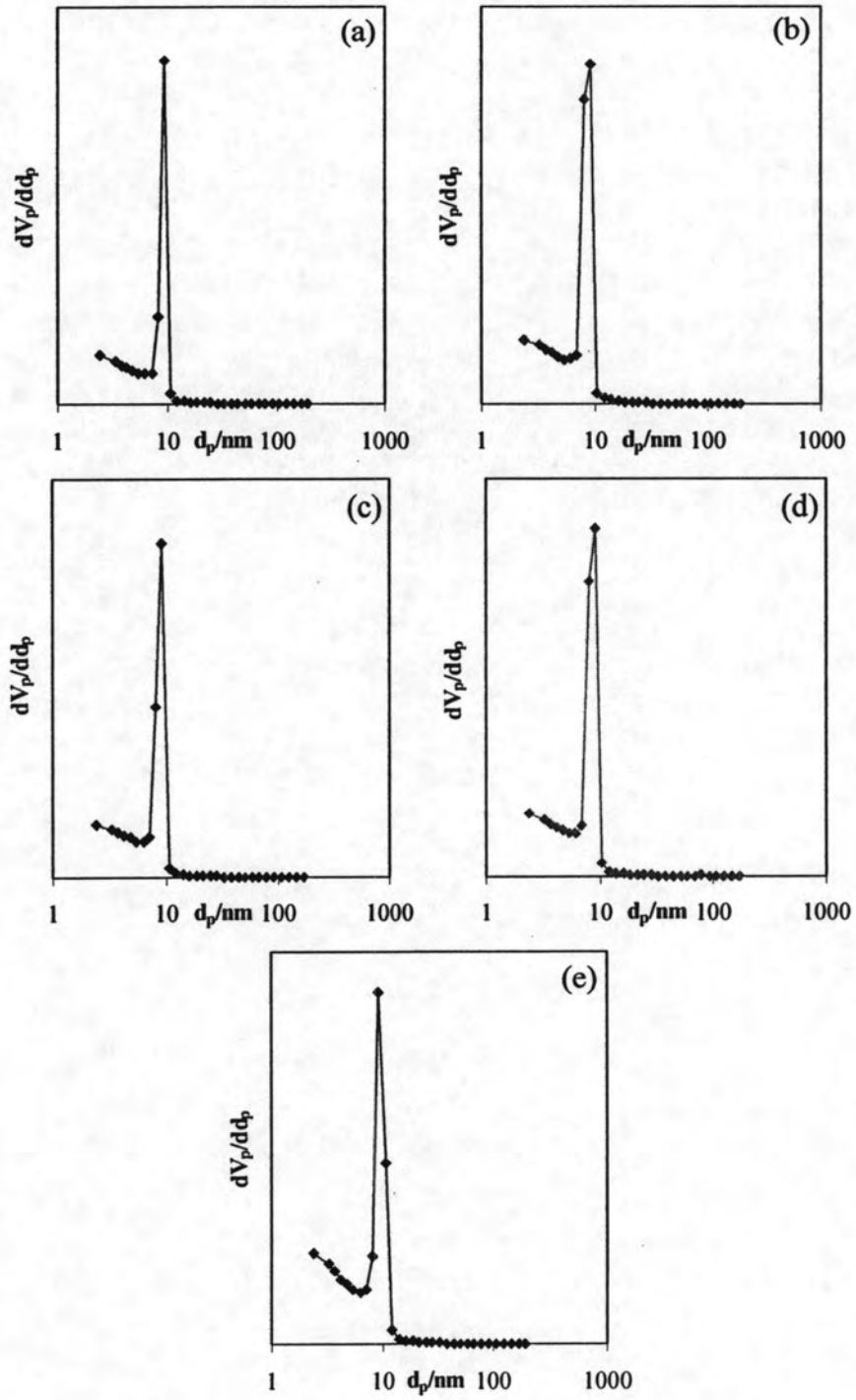

Figure 4.12 BJH-Pore size distributions of (a) SBA-15, (b) Ni-SBA-15, (c) Pt-SBA-15, (d) Pd-SBA-15 and (e) Ru-SBA-15.

4.3.3 SEM images of M-SBA-15 (M = Ni, Pt, Pd and Ru)

The SEM images of modified SBA-15 catalysts showed in Figure 4.13. All samples performed small rod aggregated particles. From metal addition, the small rod particles were a bit separated from the rope-liked agglomeration. In SEM-EDS method was used to measure the Ni, Pt, Pd and Ru loading in the supported SBA-15 which were 1.80, 1.54, 2.85 and 0.90%, respectively. The value from SEM-EDS less than the amount of metal solution loading (5 wt %) because some parts of metal still remained in solution.

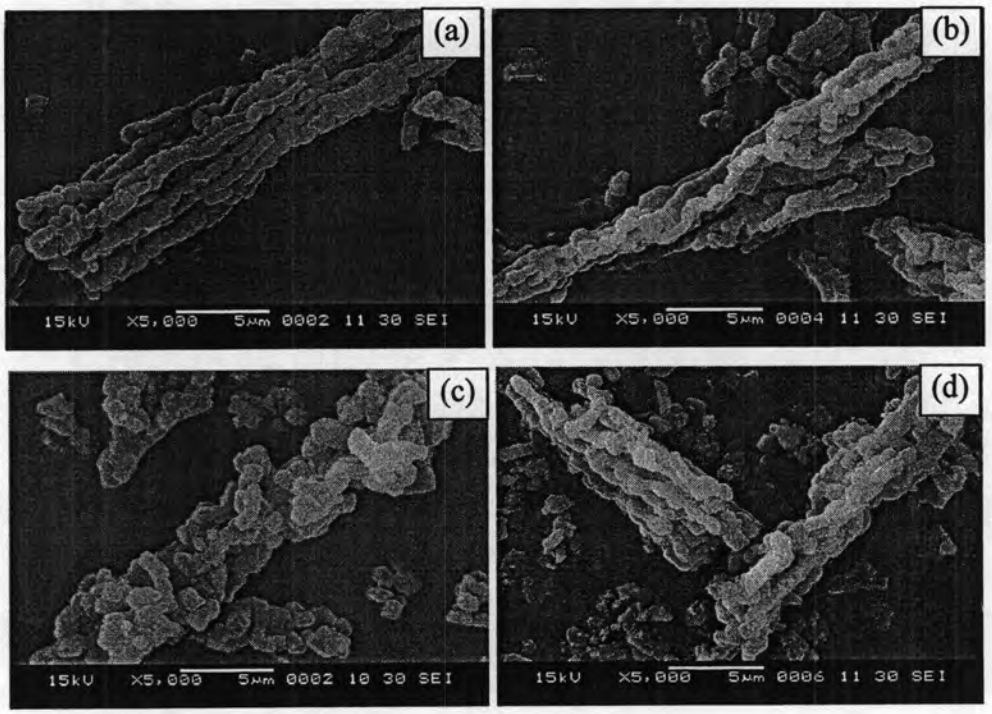

Figure 4.13 SEM images of (a) Ni-SBA-15, (b) Pt-SBA-15, (c) Pd-SBA-15 and (d) Ru-SBA-15.

4.3.4 TEM images of M-SBA-15 (M = Ni, Pt, Pd, Ru)

All the presented images of M-SBA-15 were examined by TEM showed in Figure 4.14. The TEM images proved that the location of metallic particles where placing outside the channels of the SBA-15 [15, 26]. TEM images presented the metallic particles of Ni, Pt, Pd and Ru in size 20, 10, 11 and 17 nm, respectively on the structure of SBA-15. It was cleared that these particles could not accommodate within the channels of the support, as their metallic particle size significantly exceeds the pore width of SBA-15 (estimated by the BJH method to be 9.23 nm). These results suggested that metal impregnation method could not bring in metal into the pores of SBA-15, but existed on the external surface where minority of the silanol groups located. [52]

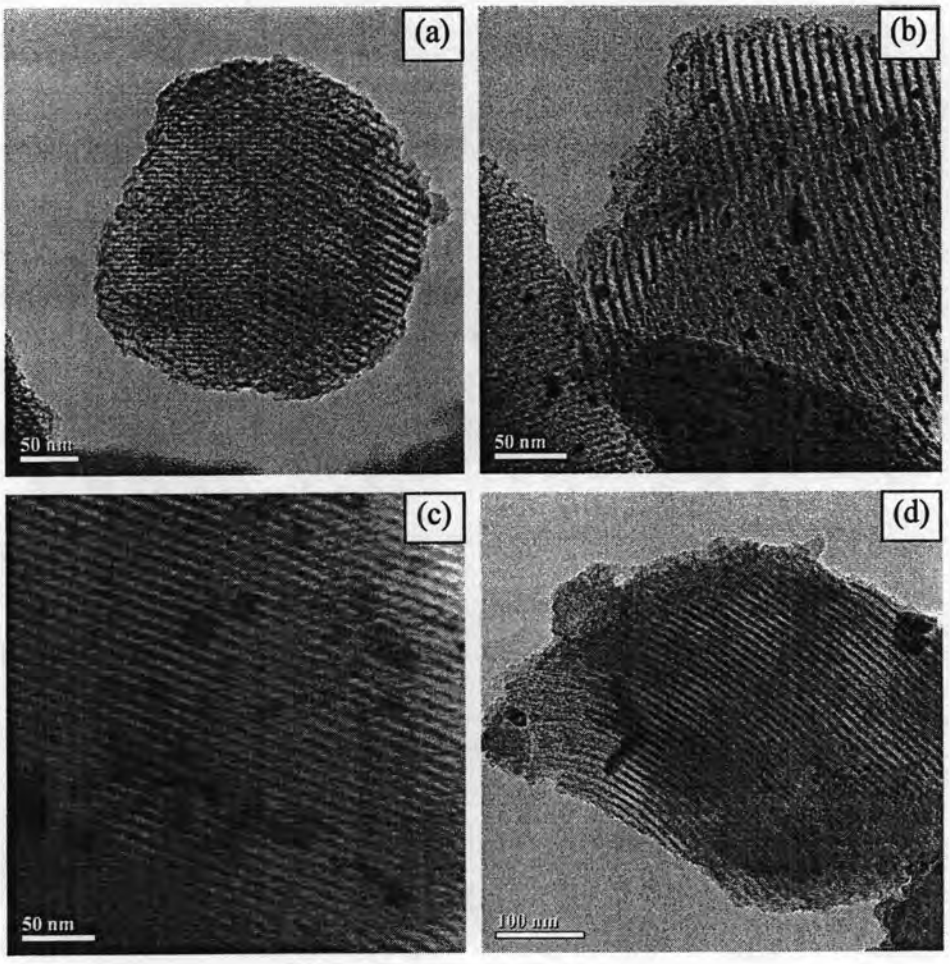

Figure 4.14 TEM images of (a) Ni-SBA-15, (b) Pt-SBA-15, (c) Pd-SBA-15 and (d) Ru-SBA-15.

4.4 The physical properties of Pd(NPs)-SBA-15

4.4.1 XRD patterns of Pd(NPs)-SBA-15

Before impregnation on supported SBA-15, Pd nanoparticles were prepared by reducing Pd^{2+} with sodium borohydride ($NaBH_4$) in β-D-glucose aqueous solution. The XRD patterns of Pd nanoparticle on supported SBA-15 (referred as Pd(NPs)-SBA-15) showed an intense peak at 0.92° and low-intensity peaks at 1.64° and 1.87°, which were attributed to hexagonal structure (Figure 4.15). The high angle XRD of Pd(NPs)-SBA-15 as Figure 4.16 showed reflections of Pd particles at 2θ = 45.4°, 66.4°, 83.9° and reflections of PdO at 2θ = 33.9°, 56.5° and 75.7° [27, 78]. In case of Pd-SBA-15 pattern showed only weak PdO peak at 2θ = 33.9°. The difference of these evidences was caused by different preparation methods. Pd-SBA-15 showed a few reflections at high angle due to the effect of chemisorption in term of Pd ions. For Pd(NPs)-SBA-15, Pd particles were formed by precipitation, then adsorbed by physisorption. Thus, Pd(NPs)-SBA-15 could perform reflection at high angle. For the peak shift might be explained as lattice parameter changed due to strain in the structure of SBA-15 by precipitated particles.

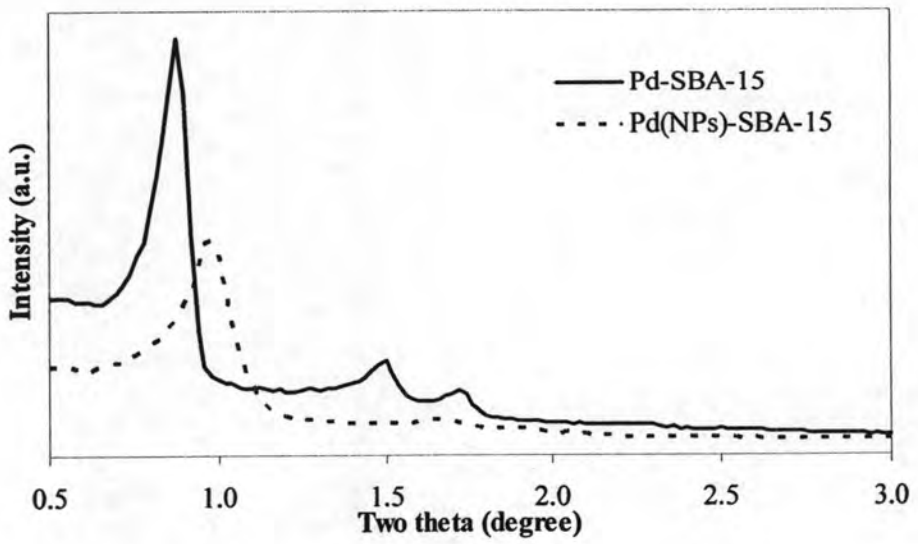

Figure 4.15 The low angle XRD patterns of Pd-SBA-15 and Pd(NPs)-SBA-15.

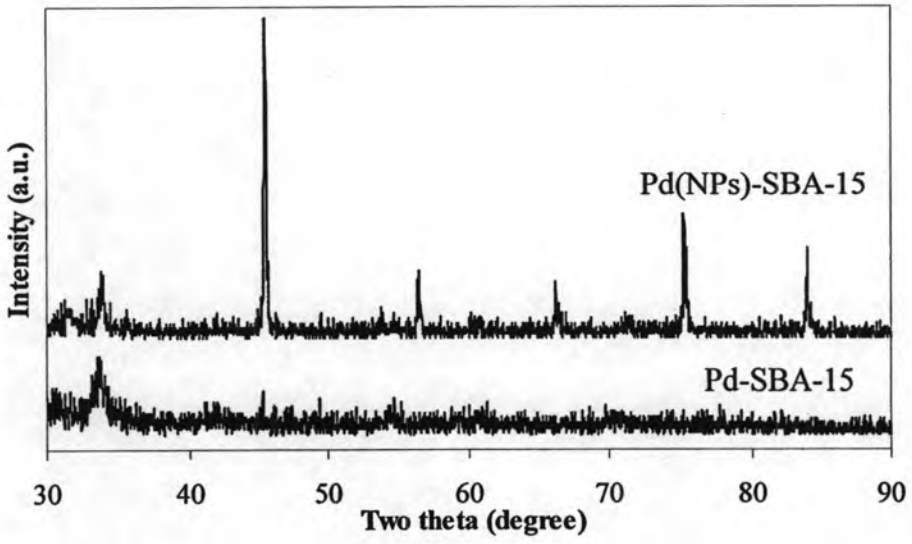

Figure 4.16 The high angle XRD patterns of Pd-SBA-15 and Pd(NPs)-SBA-15.

4.4.2 Sorption properties of Pd(NPs)-SBA-15

N_2 adsorption-desorption isotherm of Pd nanoparticles on supported SBA-15 showed in Figure 4.17. The sample performed hysteresis loop of type IV adsorption isotherm, typical for a mesoporous material. The BET specific surface area and pore size distribution showed in Figure 4.17. The surface area was found 189 m^2/g which reduced from 925 m^2/g of SBA-15. Pore size distribution was reported the same value as SBA-15 at the pore diameter of 9.23 nm. The particle size adjustment of Pd metal was estimated by TEM image to be 7 nm for Pd(NPs)-SBA-15 which diminished from 11 nm of Pd-SBA-15 some Pd particles were in the SBA-15 pore, however, partially Pd particles also located outside channels as confirmed by XRD. For this reason may cause external surface area of Pd(NPs)-SBA-15 lower than Pd-SBA-15 as that described in Section 4.3.2.

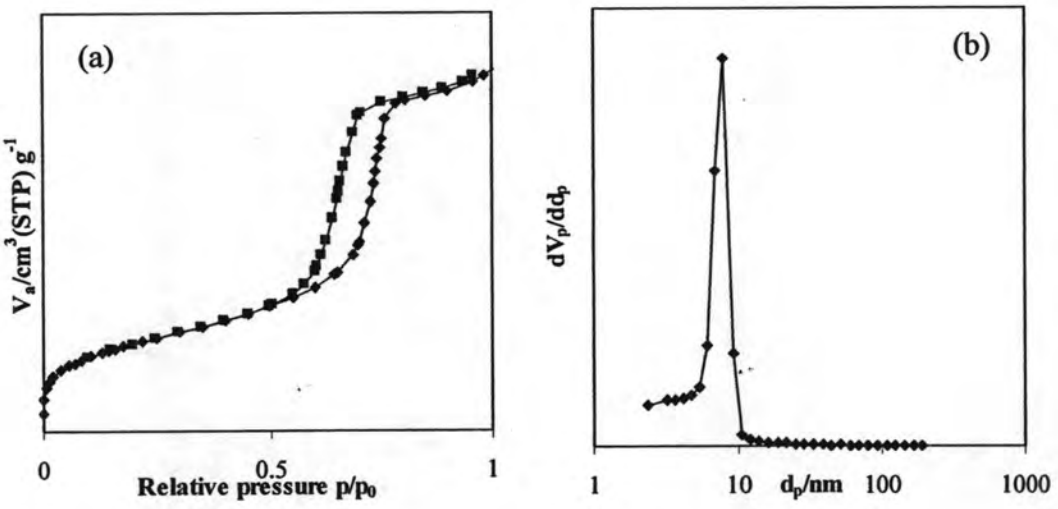

Figure 4.17 (a) N_2 adsorption-desorption isotherm and (b) BJH-pore size distribution of Pd(NPs)-SBA-15.

4.4.3 SEM images of Pd(NPs)-SBA-15

The SEM images of Pd(NPs)-SBA-15 sample showed in Figure 4.18. Pd(NPs)-SBA-15 showed small rod particles to form rope-liked agglomeration. In SEM-EDS method measured the amount of Pd metal loading in Pd(NPs)-SBA-15 describing as 2.05 %.

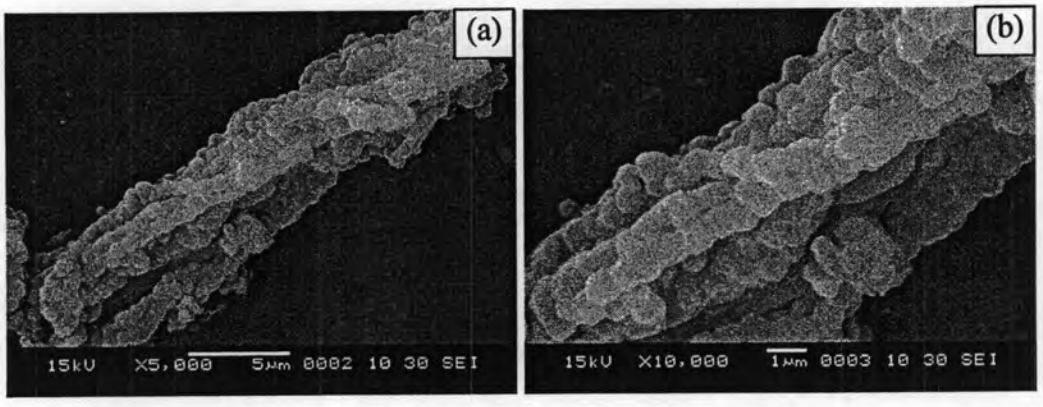

Figure 4.18 SEM images of Pd(NP)-SBA-15 at different magnifications (a) ×5,000 and (b) ×10,000.

4.4.4 TEM images of Pd(NPs)-SBA-15

The TEM images obtained from Pd(NPs)-SBA-15 showed in Figure 4.19. The majority of Pd nanoparticles presented particle size about 7 nm which reduced from 11 nm. The main Pd particles could be adapted going into the mesoporous tubes, however, minor Pd particles still located outside channels.

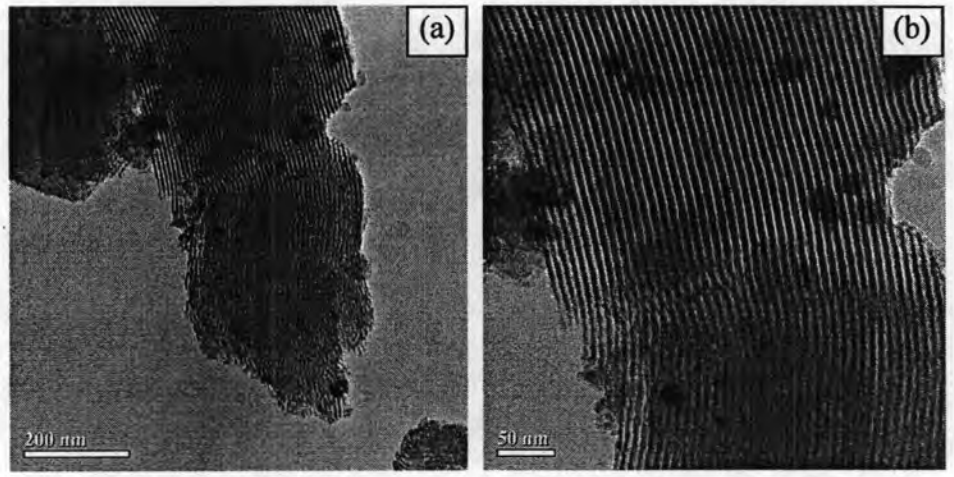

Figure 4.19 TEM images of Pd(NPs)-SBA-15 at different magnifications (a) 200 nm and (b) 50 nm.

From successfully synthetic SBA-15 derivatives, these matters were used as catalysts in pure glycerol and biodiesel waste cracking. Glycerol waste from biodiesel production contains 37.18% of glycerol and 54.48% of matter organic non-glycerol.

4.5 Pure glycerol cracking over modified SBA-15 catalysts

Figure 4.20 showed the accumulative volume of liquid fraction in the graduated cylinder obtained by catalytic cracking of pure glycerol at 400°C. This plot accounts for the kinetic rate of this reaction. For catalytic cracking and thermal cracking, the amounts of liquid in the graduated cylinder were nearly equal. From the data obtained, it was found that Pt-SBA-15 and Pd-SBA-15 catalysts showed rate of liquid fraction

formation a much faster than other catalysts at initial step. However, the overall rates of liquid fraction formation were not significantly different for each catalyst.

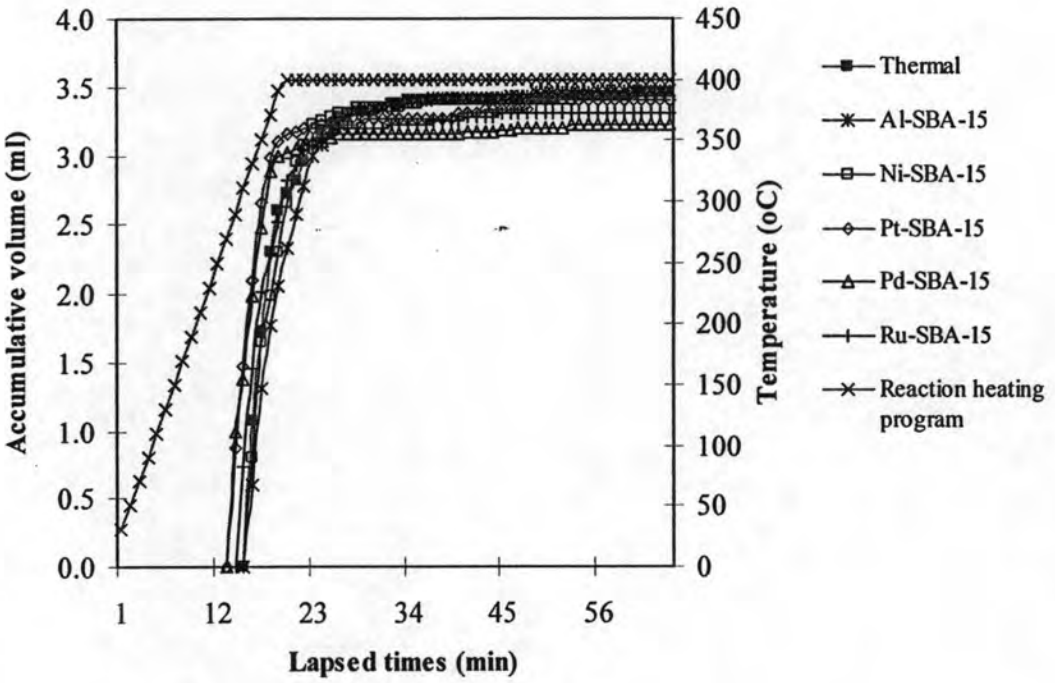

Figure 4.20 Accumulative volume of liquid fraction from thermal cracking and catalytic cracking of pure glycerol over modified SBA-15 catalysts (Condition: 10 wt% catalyst to substrate, N_2 flow to 20 ml/min, 400°C and reaction time of 40 min).

The conversion value and product yield acquired by the catalytic cracking of pure glycerol (Fluka, ≥99.5%) over Ni-SBA-15, Pt-SBA-15, Pd-SBA-15, Ru-SBA-15 and thermal cracking at 400°C were compared in Table 4.2. All catalytic reactions showed higher conversion than thermal cracking. Considering product yield, catalytic cracking of pure glycerol over all catalysts produced high amount of liquid fraction then the liquid fraction was distilled under vacuum and gave main product as heavy oil. The yields of gas fraction were in the range of 4-14% while liquid fractions were about 79-84%. The Pd-SBA-15 catalyst exhibited the highest conversion about 93%, with 14% yield of gas fraction, and 66% yield of heavy liquid fraction.

Table 4.2 Value of %conversion and %yield obtained from thermal cracking and catalytic cracking of pure glycerol over modified SBA-15 catalysts (Condition: 10 wt% catalyst to substrate, N_2 flow to 20 ml/min, 400°C and reaction time of 40 min).

	Thermal	Al-SBA-15	Ni-SBA-15	Pt-SBA-15	Pd-SBA-15	Ru-SBA-15
% Conversion[a]	87.80	89.60	90.07	92.53	93.40	89.47
% Yield[b]						
1.Gas fraction	4.00	5.67	8.33	9.47	14.13	8.40
2.Liquid fraction	83.80	83.93	81.73	82.87	79.27	81.07
- distillated liquid	7.79	9.00	12.21	15.55	12.91	9.01
- heavy liquid	76.01	74.93	69.52	67.32	66.36	72.06
3.Residue	12.20	10.40	9.93	7.47	6.60	10.53
Total volume of liquid fraction (ml)	3.45	3.47	3.40	3.40	3.22	3.30
Liquid fraction density (g/ml)	1.21	1.21	1.20	1.22	1.23	1.23

[a]*deriviation within 0.50%*
[b]*deriviation within 0.40%*

Gas product distribution from thermal and M-SBA-15 catalysts cracking of pure glycerol showed in Figure 4.21. Gas products were selective to CO_2 and propene excepted for Pd-SBA-15 catalyst produced unexpected CO as a maximum amount ~11%. These catalysts performed different product yield due to an effect of variety metals on SBA-15. Pd-SBA-15 catalyst was highly selective towards CO, whereas the CO_2 selectivity was found to be lower than other catalysts. In comparison with Fernando *et al.* report [17] that using Pd/Al_2O_3 catalyst in glycerin steam reforming gave CO as main product. This can be attributed to the primary reaction in glycerin steam reforming as in equation (1). The steam reforming reaction of glycerin proceeds according to the following equations:

$$C_3H_8O_3 \longrightarrow 3CO + 4H_2 \quad (1)$$

$$CO + H_2O \longleftrightarrow CO_2 + H_2 \quad (2)$$

$$CH_4 + H_2O \longrightarrow CO + H_2 \quad (3)$$

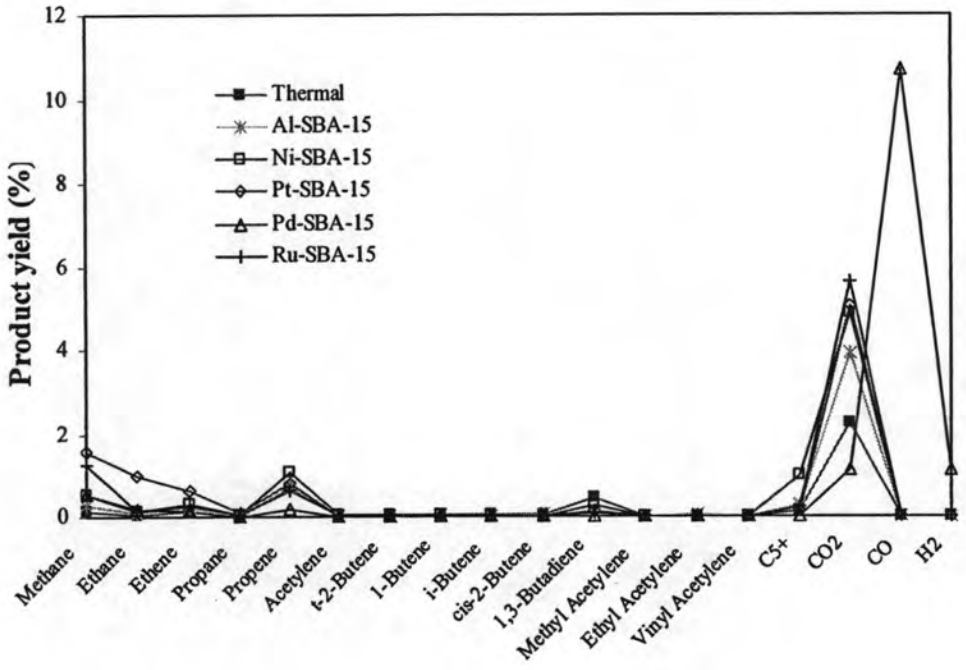

Figure 4.21 Distribution of gas fraction obtained from thermal cracking and catalytic cracking of pure glycerol over modified SBA-15 catalysts (Condition: 10 wt% catalyst to substrate, N_2 flow to 20 ml/min, 400°C and reaction time of 40 min).

The product distributions of distillated liquid obtained by thermal cracking and catalytic cracking of pure glycerol at 400°C showed in Figure 4.22. The product distributions of volatile liquid phase for all catalysts were selective to 2-propen-1-ol and 1-hydroxy-2-propanone. When the reaction temperature was risen higher than glycerol boiling point, evaporated liquid was transformed to 1-hydroxy-2-propanone *via* dehydration and tautomerization then this 1-hydroxy-2-propanone was reduced and dehydrated to 2-propen-1-ol as shown in scheme 4.1.

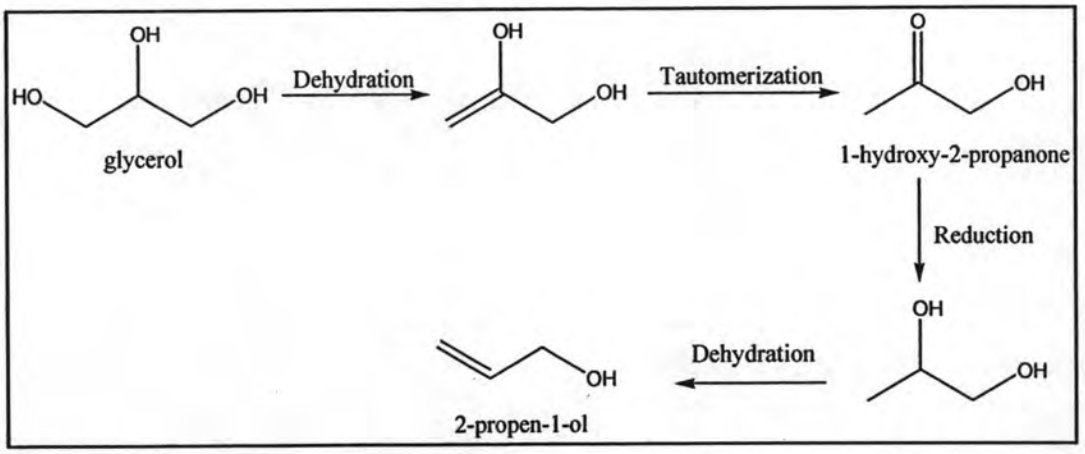

Scheme 4.1 Transformations of glycerol to product.

All catalysts promoted 2-propen-1-ol as major product except for Pd-SBA-15 catalyst produced 1-hydroxy-2-propanone as a main liquid product.

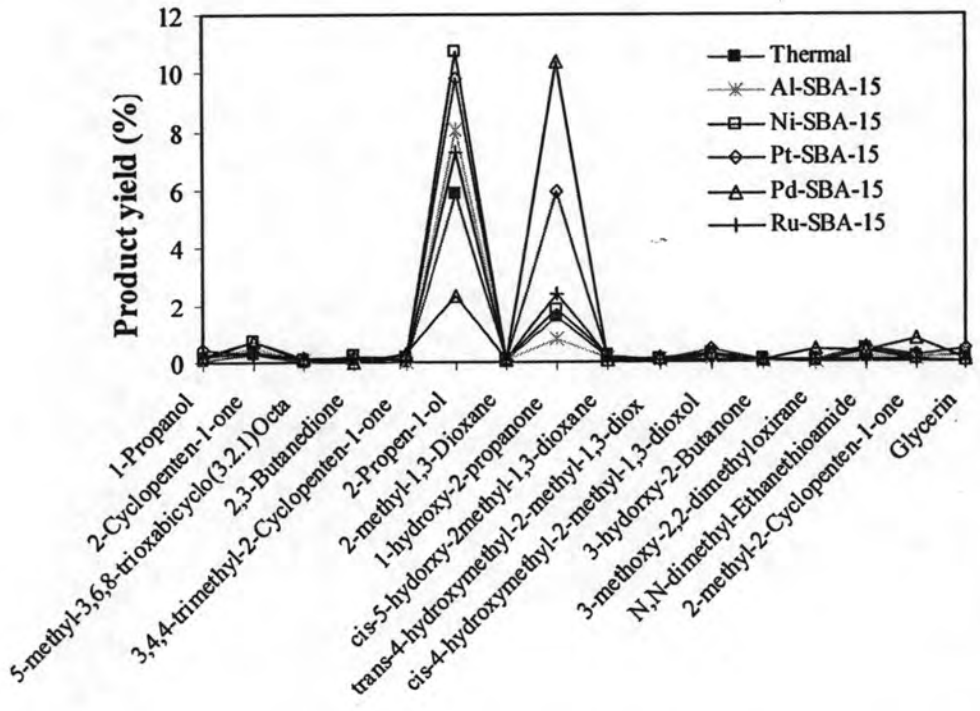

Figure 4.22 Distribution of liquid fraction obtained from thermal cracking and catalytic cracking of pure glycerol over modified SBA-15 catalysts (Condition: 10 wt% catalyst to substrate, N_2 flow to 20 ml/min, 400°C and reaction time of 40 min).

4.6 Glycerol waste cracking over Al-SBA-15 catalyst

From the pure glycerol cracking over modified SBA-15 catalysts in previous section could be conclude that catalytic cracking obtained high conversion but only heavy liquid fraction was promoted. Then from this point, glycerol waste from biodiesel production was used as starting material in the next experiments. The composition of glycerol waste was determined in order to predict cracking product. Biodiesel production waste was found out composition by using standard method [79-82]. The analysis results were showed in term of 54.48% of matter organic non-glycerol, 37.18% of glycerol, 6.49% of ash and 1.85% of water content. In addition, the density of glycerol waste was 1.03 g/ml at 20°C and pH value was 10.47 [83-84]. [85]

4.6.1 Effect of reaction temperature

The Al-SBA-15 catalyst was used for studying the effect of the reaction temperature on its activity. Figure 4.23 and 4.24 showed the volume of accumulative volume of liquid fraction in the graduated cylinder obtained by thermal cracking and catalytic cracking of glycerol waste at reaction temperatures from 400 to 800°C. This plot accounts for the kinetic rate of the liquid formation. From result, it was found that temperature 400°C exhibited rate of liquid formation slower than other higher temperatures. The kinetic rate was increased when rising reaction temperature beside the kinetic rates by catalytic cracking above thermal cracking at the same reaction temperature.

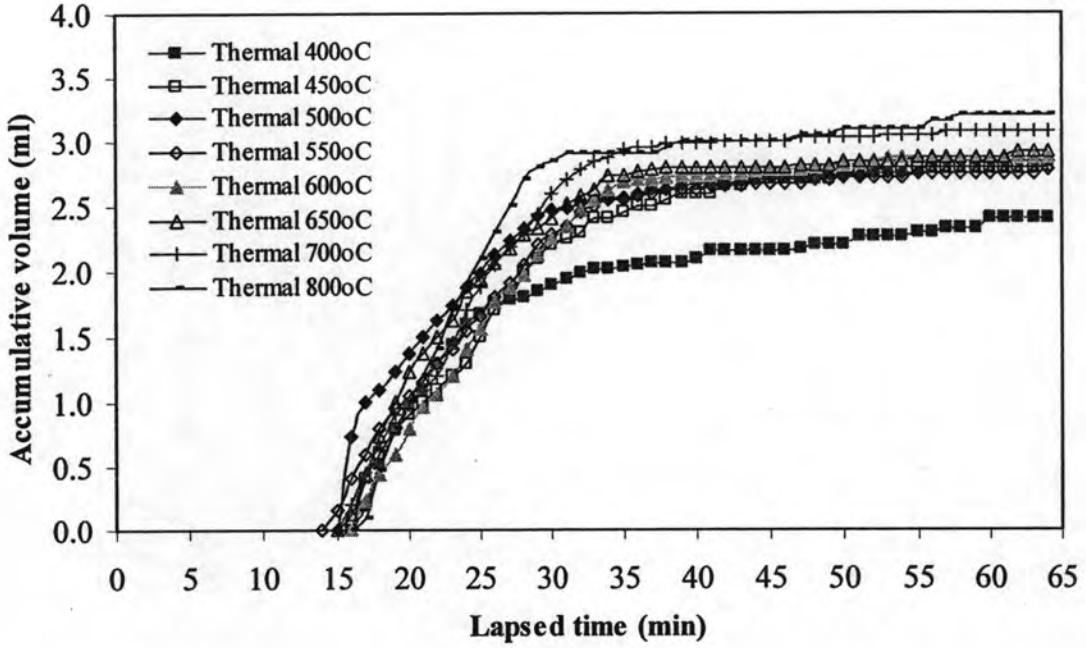

Figure 4.23 Accumulative volume of liquid fraction from thermal cracking of glycerol waste at the different reaction temperatures (Condition: 10 wt% catalyst of substrate, N_2 flow of 20 ml/min and reaction time of 40 min).

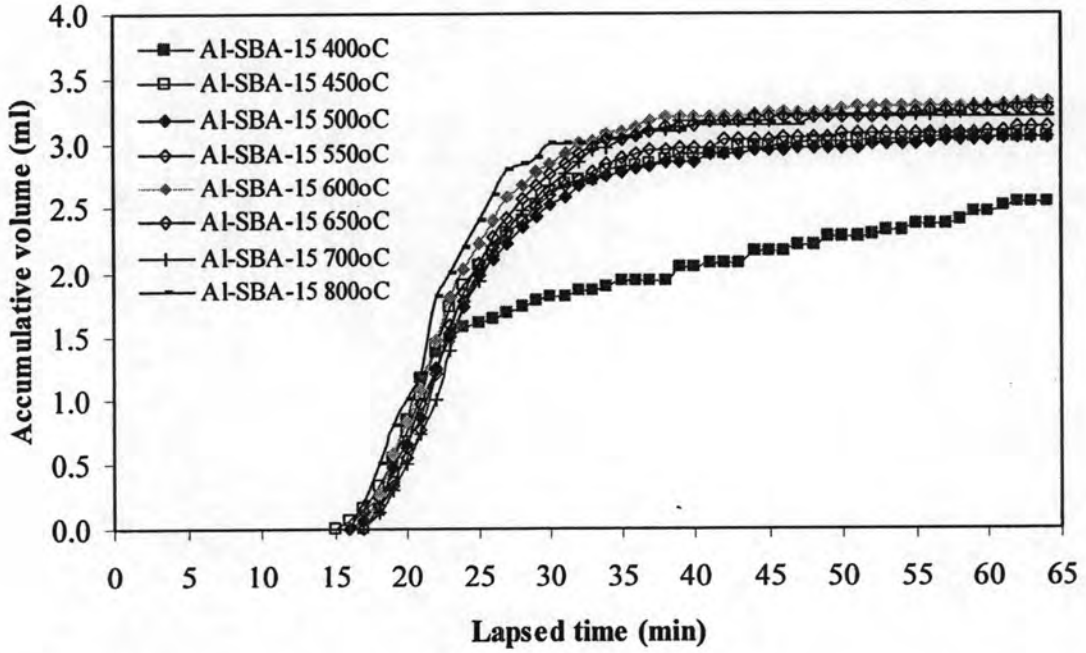

Figure 4.24 Accumulative volume of liquid fraction from Al-SBA-15 cracking of glycerol waste at the different reaction temperatures (Condition: 10 wt% catalyst of substrate, N_2 flow of 20 ml/min and reaction time of 40 min).

The conversion value and product yield of thermal cracking of glycerol waste and catalytic cracking over Al-SBA-15 were shown in Table 4.3 and 4.4. The thermal cracking in an absent of catalyst testing for comparison. The conversion of catalytic cracking was higher than thermal cracking about 3-5% at the same reaction temperature, moreover conversion increased when rising reaction temperature. Conversion values increased remarkably when reaction temperature was increased from 400 to 450 °C. For all cases when considering the reactions from 450 to 800°C, in case of thermal cracking gave liquid fraction about 51-59% whereas the cracking with Al-SBA-15 gave liquid fraction 58-62%. However in case of thermal cracking, reaction temperature at 800°C gave lower gas fraction than reaction temperature at 700°C due to deposition of wax residue at reactor sidearm, therefore that residue could not cracked in the reactor.

Table 4.3 Value of %conversion and %yield obtained from thermal cracking of glycerol waste at the different reaction temperatures (Condition: 10 wt% catalyst of substrate, N_2 flow of 20 ml/min and reaction time of 40 min)

	Reaction temperature (°C)							
	400	**450**	**500**	**550**	**600**	**650**	**700**	**800**
% Conversion[a]	63.53	82.80	81.27	81.00	83.07	84.97	88.20	86.30
% Yield[b]								
1.Gas fraction	14.53	30.40	28.93	30.00	29.67	28.23	29.70	27.30
2.Liquid fraction	49.00	52.40	52.33	51.00	53.40	56.73	58.50	59.00
- distillated liquid	22.44	16.90	20.84	22.93	23.08	23.27	25.33	23.77
- heavy liquid	26.56	35.50	31.49	28.07	30.32	33.46	33.18	35.23
3.Residue	36.47	17.20	18.73	19.00	16.93	15.13	11.80	13.70
Total volume of liquid fraction (ml)	2.40	2.80	2.75	2.80	2.93	2.97	3.15	3.23
Liquid fraction density (g/ml)	1.02	0.94	0.96	0.91	0.91	0.95	0.93	0.92

[a] *deriviation within 0.60%*
[b] *deriviation within 0.50%*

Table 4.4 Value of %conversion and %yield obtained from Al-SBA-15 cracking of glycerol waste at the different reaction temperatures (Condition: 10 wt% catalyst of substrate, N_2 flow of 20 ml/min and reaction time of 40 min).

	Reaction temperature (°C)							
	400	**450**	**500**	**550**	**600**	**650**	**700**	**800**
% Conversion[a]	62.53	84.20	83.50	86.00	88.47	86.80	86.60	88.90
% Yield[b]								
1.Gas fraction	15.53	25.20	25.40	27.90	27.53	25.60	24.33	27.30
2.Liquid fraction	47.00	58.90	58.10	58.10	60.93	61.20	62.27	61.60
- distillated liquid	18.77	22.71	23.15	25.78	25.28	25.77	25.00	22.57
- heavy liquid	28.23	36.19	34.95	29.12	35.65	35.43	37.27	39.03
3.Residue	37.47	15.80	16.50	14.00	14.60	13.20	13.40	11.10
Total volume of liquid fraction (ml)	2.53	3.18	3.13	3.13	3.38	3.35	3.43	3.33
Liquid fraction density (g/ml)	0.93	0.93	0.93	0.93	0.90	0.91	0.91	0.93

[a]deriviation within 0.40%
[b]deriviation within 0.50%

Figure 4.25 and 4.26 showed product distribution of gas fraction obtained by thermal cracking and catalytic cracking of glycerol waste over Al-SBA-15 catalyst with reaction temperatures 400-800°C. Among gas products, formation of CO_2, 1,3-butadiene methane, ethene and propene were favored, which these gases could be separated purification to reuse as raw material in petrochemical process.

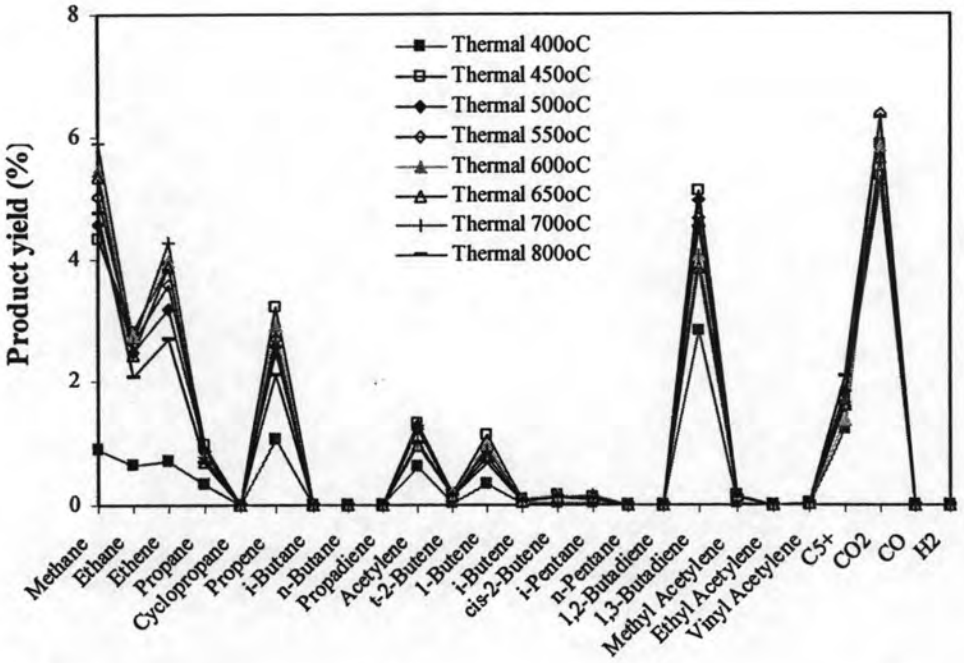

Figure 4.25 Distribution of gas fraction obtained from thermal cracking of glycerol waste at the different reaction temperatures (Condition: 10 wt% catalyst of substrate, N_2 flow of 20 ml/min and reaction time of 40 min).

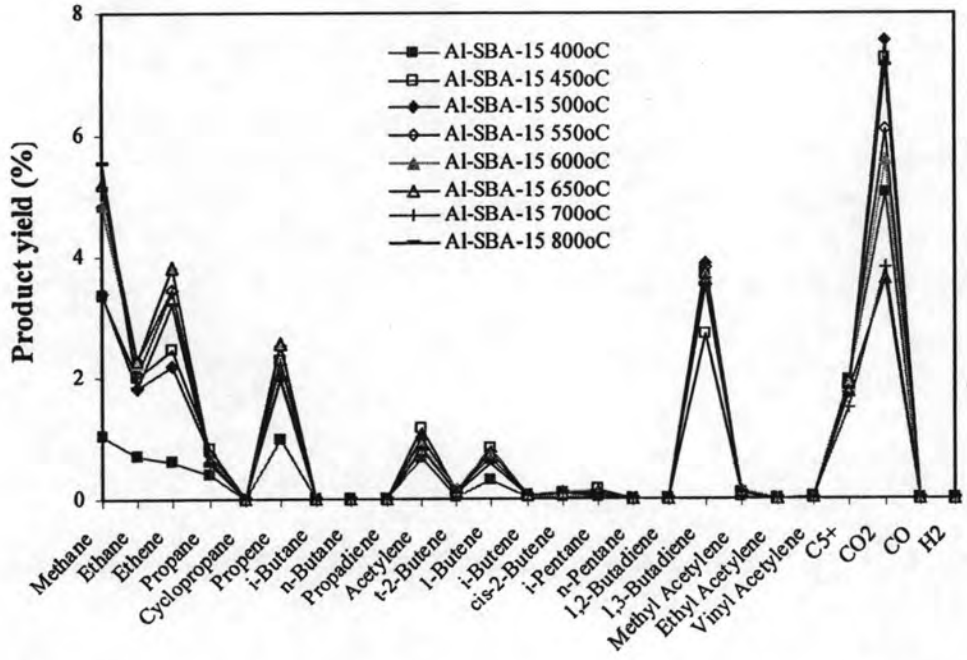

Figure 4.26 Distribution of gas fraction obtained from Al-SBA-15 cracking of glycerol waste at the different reaction temperatures (Condition: 10 wt% catalyst of substrate, N_2 flow of 20 ml/min and reaction time of 40 min).

Figure 4.27 and 4.28 showed product distribution of distillated liquid obtained by thermal cracking and catalytic cracking. The cracking product composition depends on reaction temperature and catalytic effects. However, thermal cracking gave 2-propen-1-ol higher than 2-cyclopenten-1-one. On the other hands, in case of using Al-SBA-15, 2-cyclopenten-1-one was promoted at reaction temperature higher than 600°C which 2-cyclopenten-1-one used in the industrial production for perfumes and agricultural chemical.

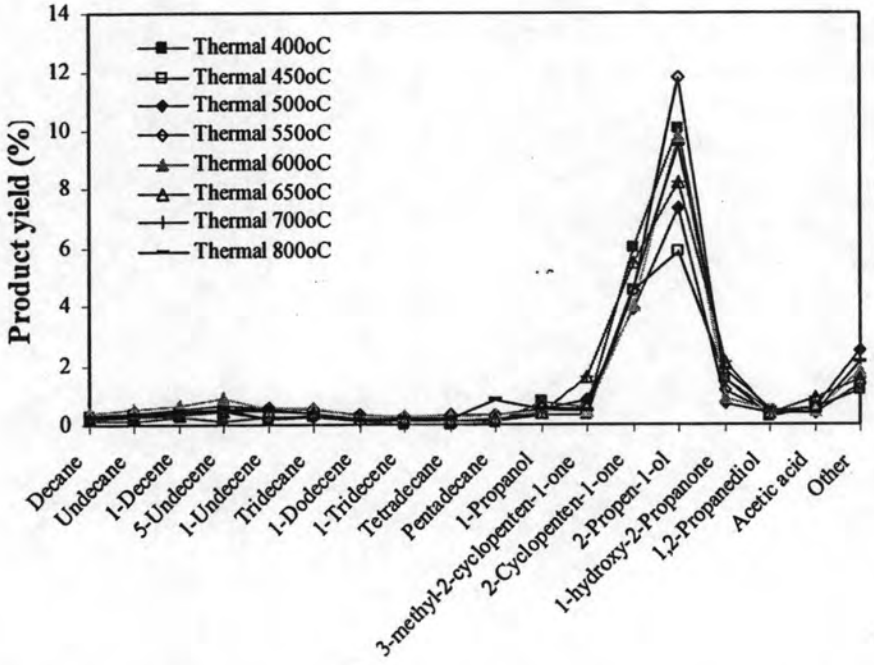

Figure 4.27 Distribution of liquid fraction obtained from thermal cracking of glycerol waste at the different reaction temperatures (Condition: 10 wt% catalyst of substrate, N_2 flow of 20 ml/min and reaction time of 40 min).

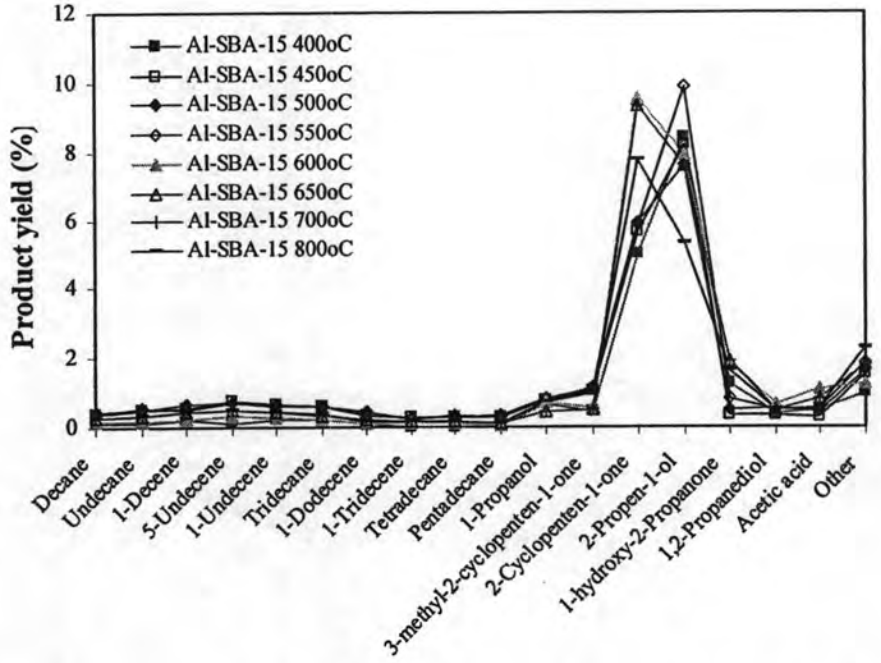

Figure 4.28 Distribution of liquid fraction obtained from Al-SBA-15 cracking of glycerol waste at the different reaction temperatures (Condition: 10 wt% catalyst of substrate, N_2 flow of 20 ml/min and reaction time of 40 min).

4.7 Glycerol waste cracking over metal on supported SBA-15 catalysts

In previous parts glycerol waste from biodiesel production was cracked over Al-SBA-15. From this point, metal on supported SBA-15 materials, *i.e.* Ni-SBA-15, Pt-SBA-15, Pd-SBA-15 and Ru-SBA-15, were introduced to utilize as catalyst in biodiesel production waste cracking. For compared its catalytic activities and selectivities.

4.7.1 Effect of reaction temperature

The accumulative volume of liquid fraction in the graduated cylinder obtained by cracking of glycerol waste over Ni, Pt, Pd and Ru on SBA-15 at temperatures 400, 650 and 800°C showed in Figure 4.29 to Figure 4.31. The initial rate of liquid formation, there were no significant difference for all catalysts at all reaction temperatures. The total volume of liquid fraction produced in range 45-61%.

At reaction temperature 650°C, the Ni-SBA-15 produced liquid product faster than other catalysts while Pd-SBA-15 and Ru-SBA-15 gave high product selectivity of gas and distillated liquid, respectively. Then, next reaction at 800°C only Pd-SBA-15 and Ru-SBA-15 were tested for catalytic cracking.

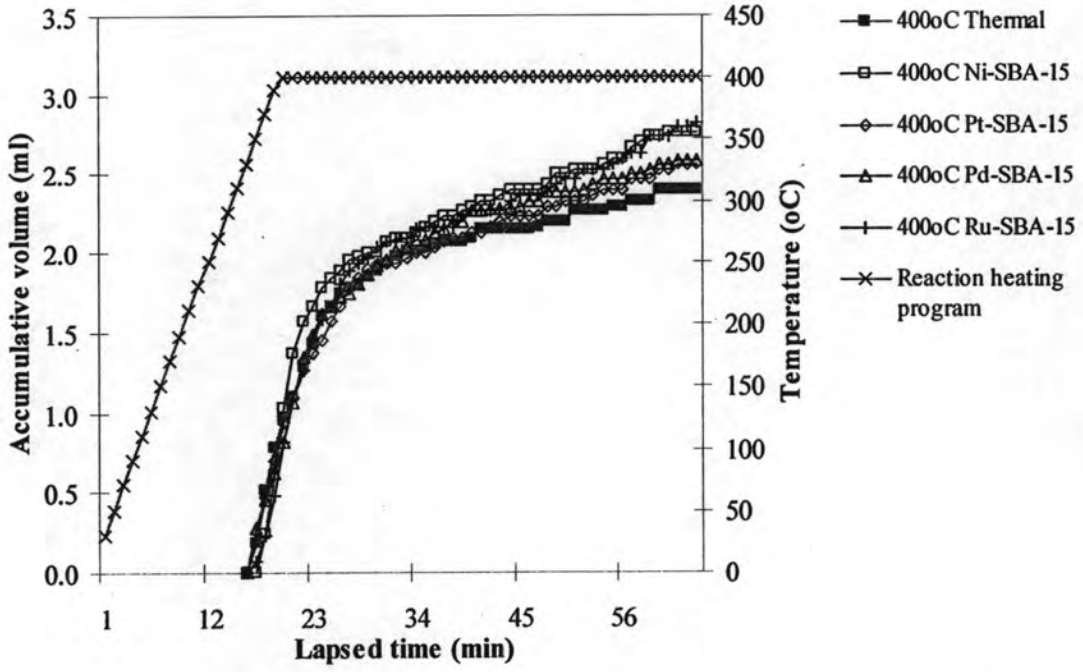

Figure 4.29 Accumulative volume of liquid fraction from catalytic cracking of glycerol waste over Ni, Pt, Pd and Ru on supported SBA-15 catalysts (Condition: N_2 flow of 20 ml/min, 400°C and reaction time of 40 min).

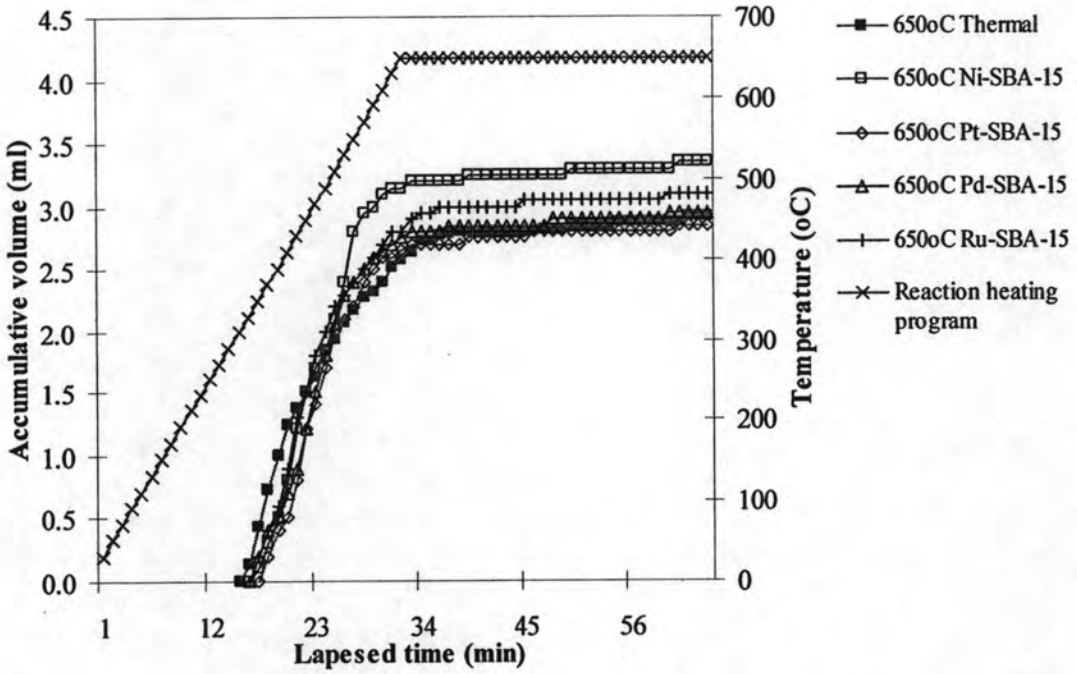

Figure 4.30 Accumulative volume of liquid fraction from catalytic cracking of glycerol waste over Ni, Pt, Pd and Ru on supported SBA-15 catalysts (Condition: N_2 flow of 20 ml/min, 650°C and reaction time of 40 min).

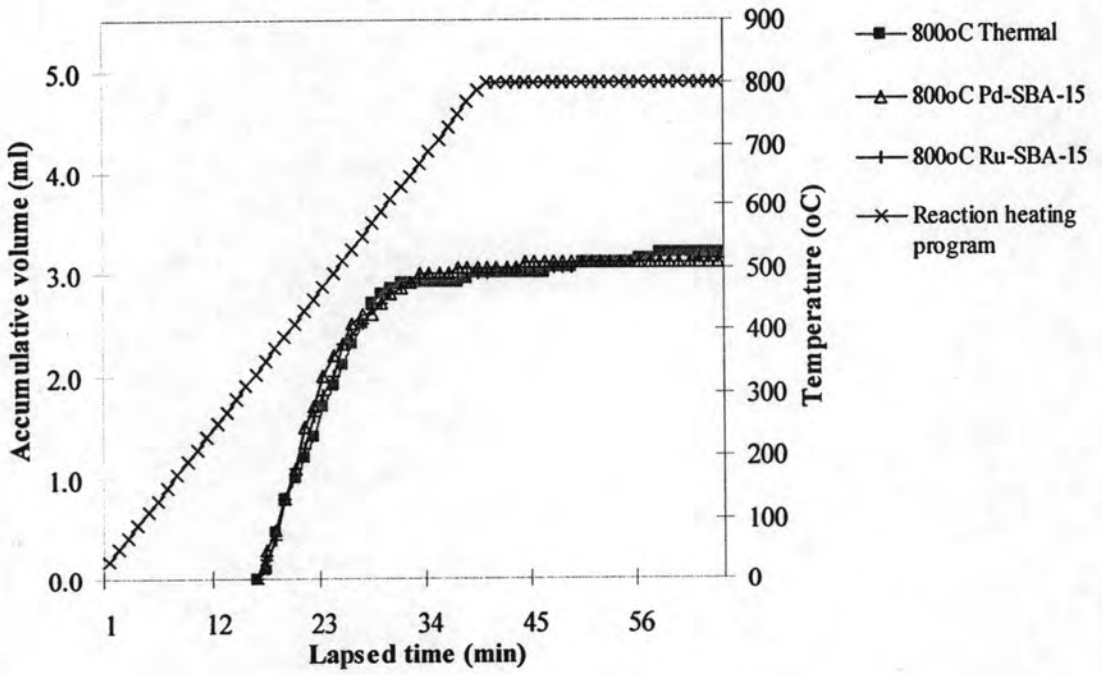

Figure 4.31 Accumulative volume of liquid fraction from catalytic cracking of glycerol waste over Pd and Ru on supported SBA-15 catalysts (Condition: N_2 flow of 20 ml/min, 800°C and reaction time of 40 min).

The conversion and product yield of thermal cracking and catalytic cracking over metal supported SBA-15 catalysts at temperature 400, 650 and 800°C were shown in Table 4.5 to 4.7. M-SBA-15 catalysts were used for studying the effect of temperature and catalyst type. Conversion values increase when reaction temperature was increased. The conversion significantly was affected by temperature increasing from 400 to 650°C. At reaction temperature 400°C, conversions were in range 63-71% while conversions were increased to 84-88% at reaction temperature 650°C. When reaction temperature was risen to 800°C, the Pd-SBA-15 catalyst could push the conversion up to 89 %. The amount of residue was reduced to 11 wt%. When considering the reactions at 650°C and 800°C, the activities of M-SBA-15 catalysts did not show a significantly different conversion (84-89%). The conversion and product composition were slightly different when compared between catalysts. Furthermore, when reaction temperature was increased, the residue was decreased. The result indicated that residue might decompose to relatively heavy liquid fraction. When temperature was risen from 400 to 650°C, smaller liquid molecules were increased from large molecules cracking. This result corresponds to Witchakorn *et al.* [11] which conversion and small molecules of waste pyrolysis increased when rising reaction temperature.

Table 4.5 Value of %conversion and %yield obtained from catalytic cracking of glycerol waste over Ni, Pt, Pd and Ru on supported SBA-15 catalysts (Condition: N_2 flow of 20 ml/min, 400°C and reaction time of 40 min)

	Thermal	Ni-SBA-15	Pt-SBA-15	Pd-SBA-15	Ru-SBA-15
% Conversion[a]	63.53	67.67	70.93	69.53	71.67
% Yield[b]					
1.Gas fraction	14.53	17.33	25.00	25.13	19.87
2.Liquid fraction	49.00	50.33	45.93	45.40	51.80
- distillated liquid	22.44	19.90	17.02	15.14	19.12
- heavy liquid	26.56	30.44	28.92	30.26	32.68
3.Residue	36.47	32.33	29.07	29.47	28.33
Total volume of liquid fraction (ml)	2.40	2.73	2.57	2.58	2.82
Liquid fraction density (g/ml)	1.02	0.92	0.89	0.88	0.92

[a]*deriviation within 0.40%*
[b]*deriviation within 0.50%*

Table 4.6 Value of %conversion and %yield obtained from catalytic cracking of glycerol waste over Ni, Pt, Pd and Ru on supported SBA-15 catalysts (Condition: N_2 flow of 20 ml/min, 650°C and reaction time of 40 min)

	Thermal	Ni-SBA-15	Pt-SBA-15	Pd-SBA-15	Ru-SBA-15
% Conversion[a]	84.97	88.60	85.40	86.80	85.40
% Yield[b]					
1.Gas fraction	28.23	27.20	31.80	33.20	26.20
2.Liquid fraction	56.73	61.40	53.60	53.60	59.20
- distillated liquid	23.27	23.58	15.88	18.29	24.99
- heavy liquid	33.46	37.82	37.72	35.31	34.21
3.Residue	15.13	11.40	14.60	13.20	14.60
Total volume of liquid fraction (ml)	2.97	3.45	3.00	3.00	3.30
Liquid fraction density (g/ml)	0.95	0.89	0.89	0.89	0.90

[a]*deriviation within 0.60%*
[b]*deriviation within 0.50%*

Table 4.7 Value of %conversion and %yield obtained from catalytic cracking of glycerol waste over Pd and Ru on supported SBA-15 catalysts (Condition: N_2 flow of 20 ml/min, 800°C and reaction time of 40 min)

	Thermal	**Pd-SBA-15**	**Ru-SBA-15**
% Conversion[a]	86.30	89.20	86.60
% Yield[b]			
1.Gas fraction	27.30	31.00	26.00
2.Liquid fraction	59.00	58.20	60.60
- distillated liquid	23.77	20.91	23.39
- heavy liquid	35.23	37.29	37.21
3.Residue	13.70	10.80	13.40
Total volume of liquid fraction (ml)	3.20	3.20	3.30
Liquid fraction density (g/ml)	0.92	0.91	0.93

[a]deriviation within 0.40%
[b]deriviation within 0.50%

Among gas products, formation of CO_2, CO, C5+ and 1,3-butadiene were favored. The composition of cracking products depend on reaction temperature and catalytic effect showed in Figure 4.32 to 4.34. In catalytic cracking process exhibited CO and CO_2 as the main gases due to the large molecules breaking into small containing oxygen molecules. The product distributions derived from metal supported SBA-15 could create different active sites comparing to thermal reactions.

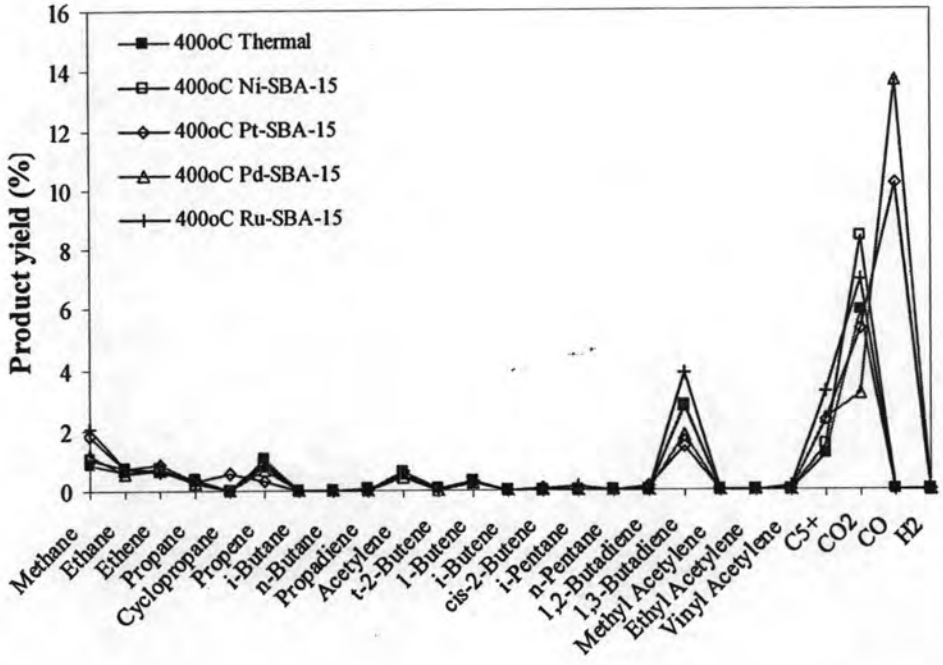

Figure 4.32 Distribution of gas fraction obtained from catalytic cracking of glycerol waste over Ni, Pt, Pd and Ru on supported SBA-15 catalysts (Condition: N_2 flow of 20 ml/min, 400°C and reaction time of 40 min)

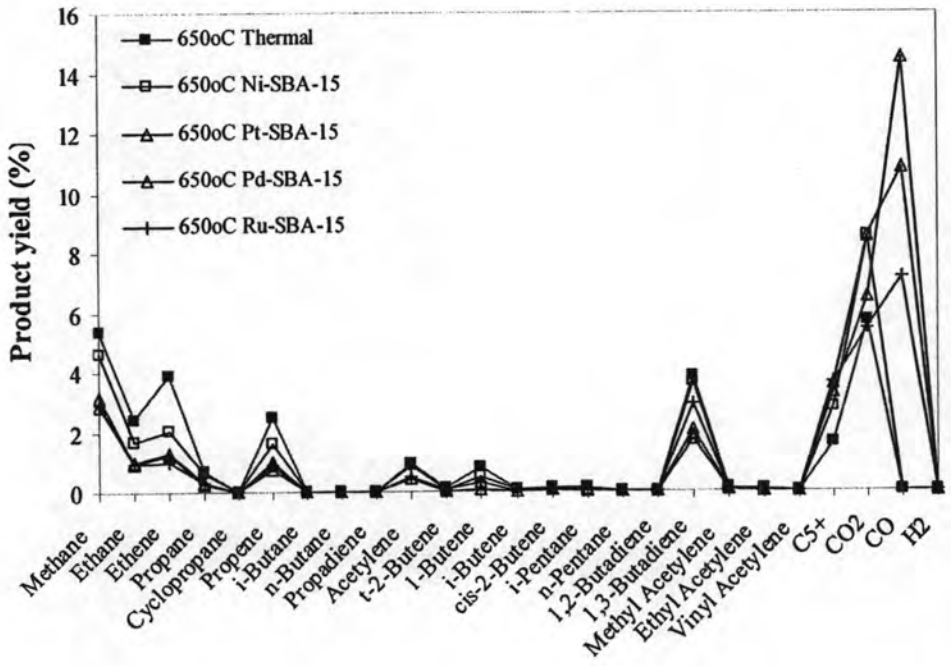

Figure 4.33 Distribution of gas fraction obtained from catalytic cracking of glycerol waste over Ni, Pt, Pd and Ru on supported SBA-15 catalysts (Condition: N_2 flow of 20 ml/min, 650°C and reaction time of 40 min).

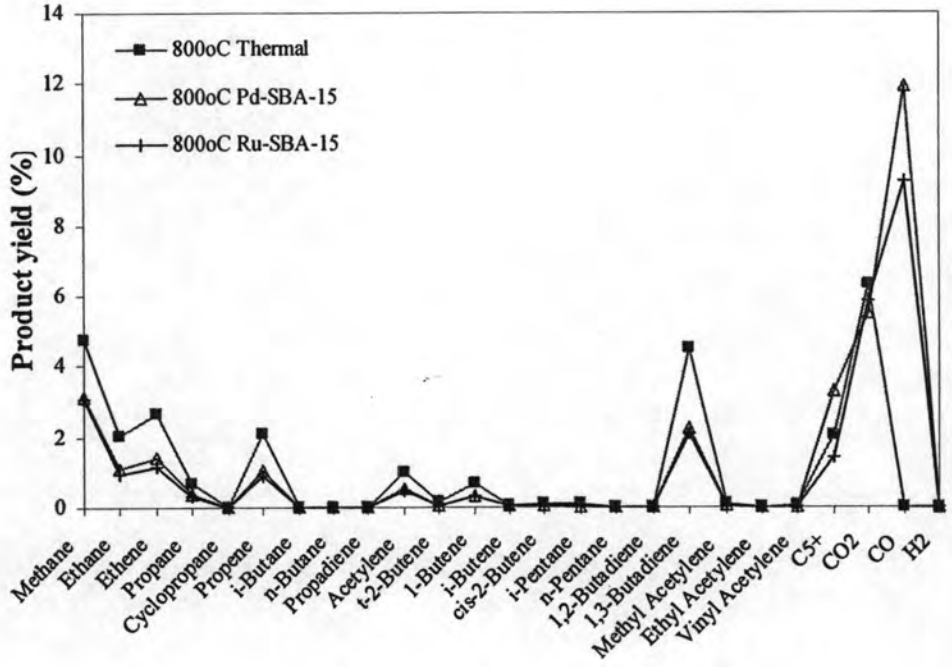

Figure 4.34 Distribution of gas fraction obtained from catalytic cracking of glycerol waste over Pd and Ru on supported SBA-15 catalysts (Condition: N_2 flow of 20 ml/min, 800°C and reaction time of 40 min).

Liquid fractions in Figure 4.35 to 4.37 showed product distribution of distillated liquid obtained by thermal cracking and catalytic cracking of glycerol waste over M-SBA-15 catalysts with three reaction temperatures at 400, 650 and 800°C. The composition of cracking products depends on reaction temperature and catalytic effect. However, thermal cracking gave 2-propen-1-ol higher than 2-cyclopenten-1-one in all cases. On the other hands, in case of M-SBA-15 catalysts, 2-cyclopenten-1-one was promoted at all reaction temperatures higher than 650°C, which could be produced from non-glycerol organic matter to cyclic ketone five membered rings.

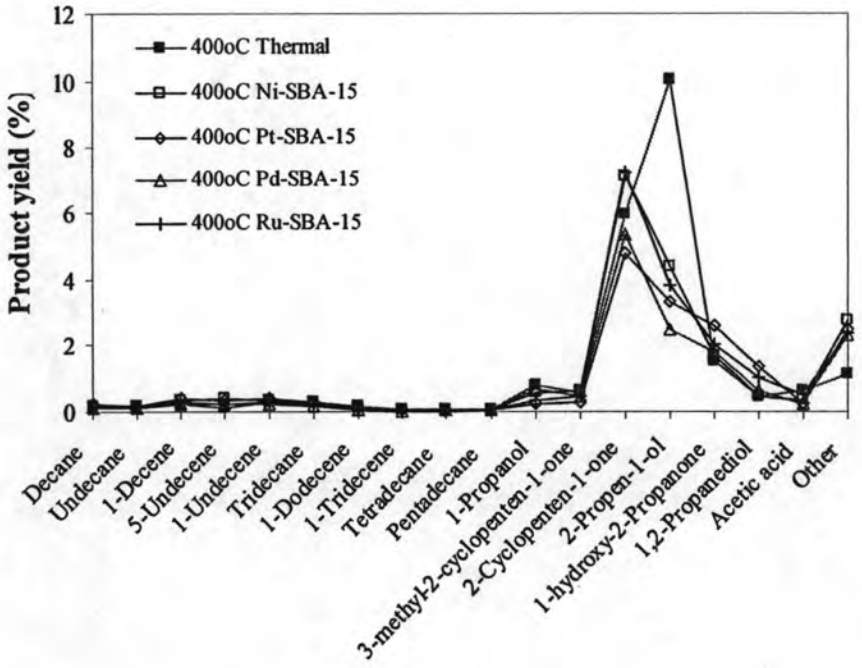

Figure 4.35 Distribution of liquid fraction obtained from catalytic cracking of glycerol waste over Ni, Pt, Pd and Ru on supported SBA-15 catalysts (Condition: N_2 flow of 20 ml/min, 400°C and reaction time of 40 min).

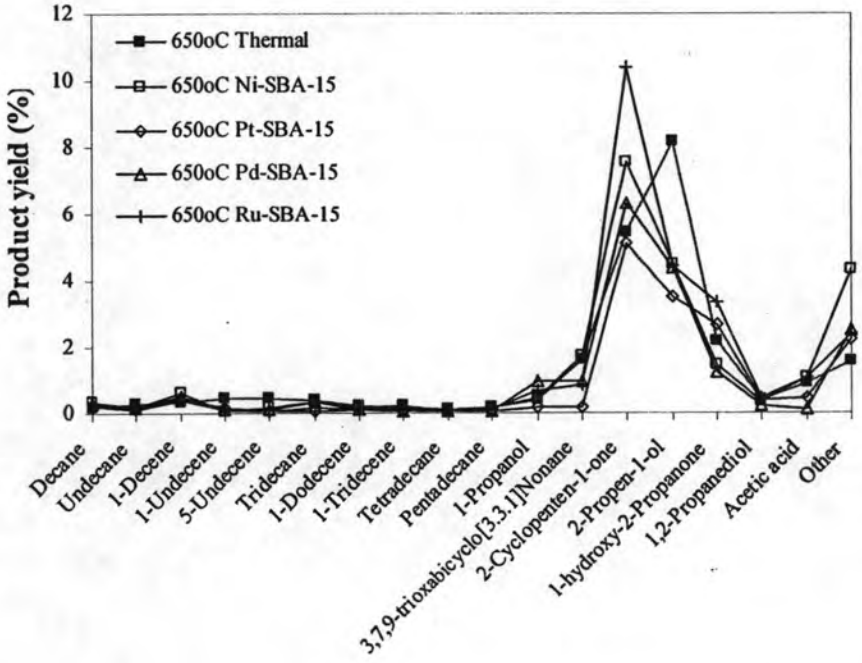

Figure 4.36 Distribution of liquid fraction obtained from catalytic cracking of glycerol waste over Ni, Pt, Pd and Ru on supported SBA-15 catalysts (Condition: N_2 flow of 20 ml/min, 650°C and reaction time of 40 min).

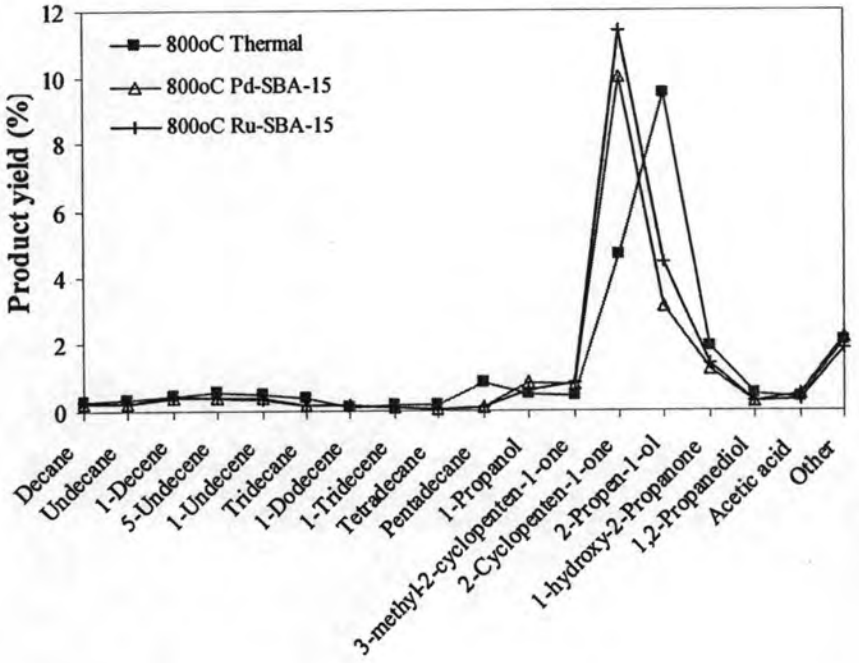

Figure 4.37 Distribution of liquid fraction obtained from catalytic cracking of glycerol waste over Pd and Ru on supported SBA-15 catalysts (Condition: N_2 flow of 20 ml/min, 800°C and reaction time of 40 min).

Pd-SBA-15 catalyst exhibited good catalytic activity for syn-gas CO producing at high selectivity above 14% at 650°C. In addition, all distribution plots of cracking products performed different product distribution, affected by variation of reaction temperature and catalyst type. Ru-SBA-15 catalyst gave 2-cyclopenten-1-one higher than other catalysts at every reaction temperatures. In thermal cracking provided 2-propen-1-ol more than catalytic cracking at all reaction temperatures especially at 400°C. From the data, the Pd-SBA-15 catalyst and reaction temperature at 650°C were chosen to study other reaction parameters according to its highest yield of gas fraction.

4.7.2 Effect of glycerol waste to catalyst ratio

The kinetic rate in catalytic cracking of glycerol waste over Pd-SBA-15 at three catalytic amounts of 5 wt%, 10 wt% and 15 wt% to glycerol waste showed in

Figure 4.38. Comparing to the kinetic rate of reactions using 5 wt%, 10 wt% and 15 wt% catalyst amounts, they exposed the same kinetic rate of liquid fraction. Upon prolongation the slope was different since 19 minute, indicated the predominant competitive rate of liquid molecules dissociation to gas molecules for catalytic amount 10 wt% and 15 wt% reactions. As a result, the total of liquid fraction in the case of 5 % catalytic amount was relatively higher than other cases.

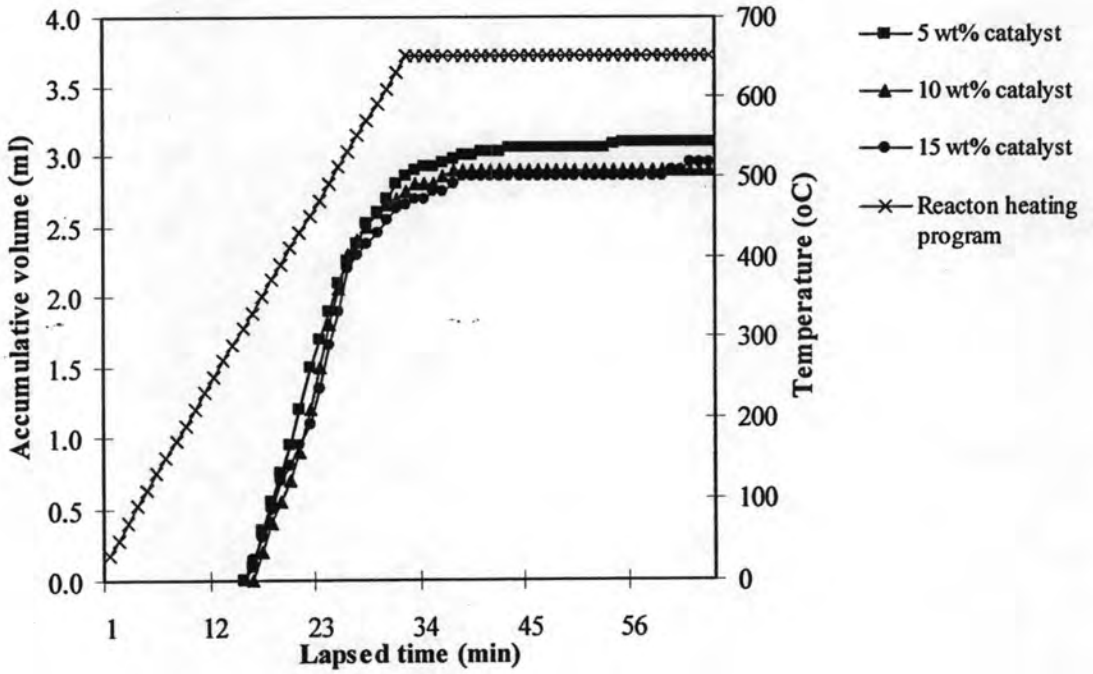

Figure 4.38 Accumulative volume of liquid fraction from Pd-SBA-15 cracking of glycerol waste at various catalyst amounts (Condition: N_2 flow of 20 ml/min, 650°C and reaction time of 40 min).

The conversion value and product yield from glycerol waste cracking over Pd-SBA-15 at various catalyst amounts were shown in Table 4.8. The conversion values nearly 86-87% were observed. The conversion depends on the catalytic amount, at high amount of catalyst further made the liquid fraction undergo cracking to smaller molecules of gas products. The amount of residue and the conversion inversely related.

Table 4.8 Value of %conversion and %yield obtained from Pd-SBA-15 cracking of glycerol waste at various catalyst amounts (Condition: N_2 flow of 20 ml/min, 650°C and reaction time of 40 min)

	Catalyst amounts to glycerol waste		
	5 wt%	**10 wt%**	**15 wt%**
% Conversion[a]	85.70	86.80	86.90
% Yield[b]			
1.Gas fraction	26.40	33.20	32.20
2.Liquid fraction	59.30	53.60	54.70
- distillated liquid	20.28	18.29	18.85
- heavy liquid	39.02	35.31	35.85
3.Residue	14.30	13.20	13.10
Total volume of liquid fraction (ml)	3.30	3.00	3.05
Liquid fraction density (g/ml)	0.90	0.89	0.90

[a]*deriviation within 0.60%*
[b]*deriviation within 0.50%*

Gas and liquid products distributions from glycerol waste cracking catalyzed by Pd-SBA-15 at various catalytic amounts presented in Figure 4.39 and 4.40, respectively. The favored gaseous products were CO, CO_2, 1,3-butadiene, C5+ and methane. The selectivity of gas fraction for 10% and 15% catalytic amounts were related but different from the reaction of 5% catalytic amount. When 5% of catalyst was used the gas product obtained only 26% and selective to CO_2, 1,3-butadiene, methane, ethene and propene. In addition at all catalytic amounts, the distillated liquid product selectivities were no significant changed. The favored liquid products were 2-cyclopropen-1-one and 2-propen-1-ol. Thus the product distribution depends on the catalyst amount. From this study, the catalytic amount 10 wt% was chosen to be used for next experiments according to obtain the highest yield of gas fraction.

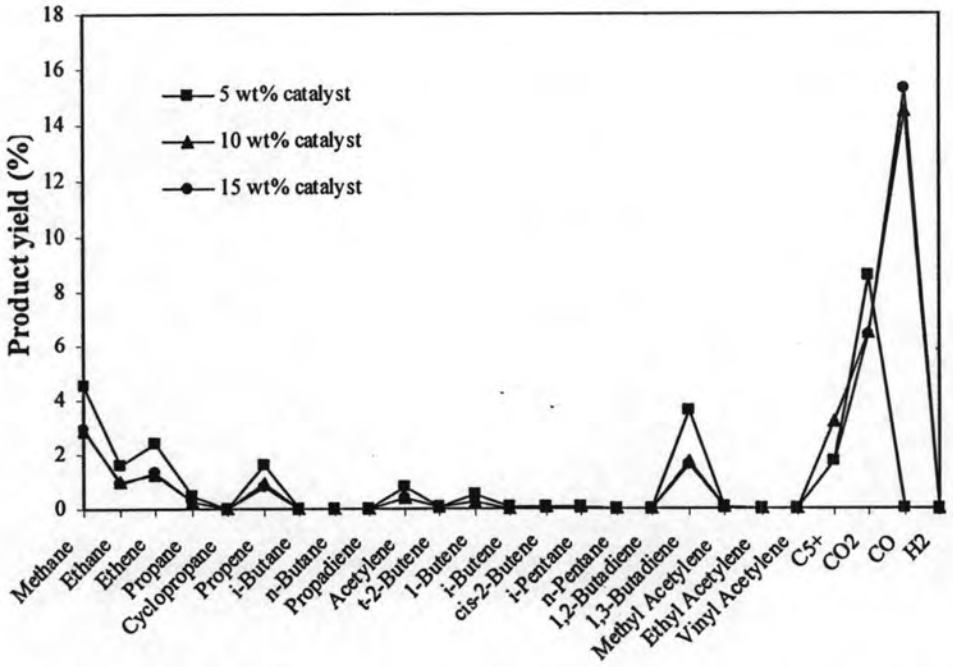

Figure 4.39 Distribution of gas fraction obtained from Pd-SBA-15 cracking of glycerol waste at various catalyst amounts (Condition: N_2 flow of 20 ml/min, 650°C and reaction time of 40 min).

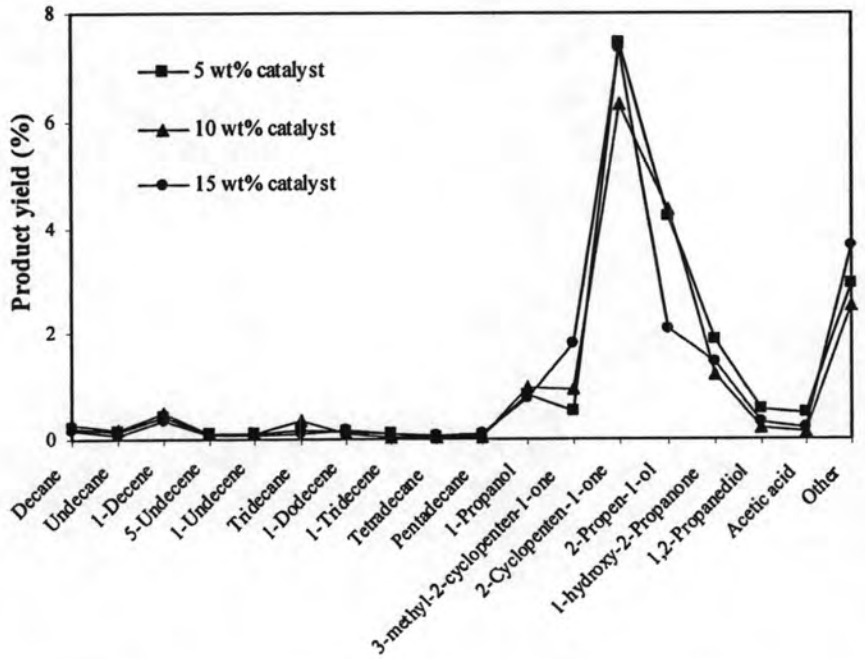

Figure 4.40 Distribution of liquid fraction obtained from Pd-SBA-15 cracking of glycerol waste at various catalyst amounts (Condition: N_2 flow of 20 ml/min, 650°C and reaction time of 40 min).

4.7.3 Effect of particle size of Pd on supported SBA-15

The kinetic rates in catalytic cracking of glycerol waste over Pd-SBA-15 with two particle sizes of Pd were compared at reaction temperature 650°C and 10 wt% of catalyst showed in Figure 4.41. At initial rate (0-34 min), both catalysts exposed the same kinetic rate of liquid fraction. As a result, the total of liquid fraction in the case of Pd(NPs)-SBA-15 catalyst (Pd in size 7 nm) is relatively higher than that in case of Pd-SBA-15 catalyst (Pd in size 11 nm).

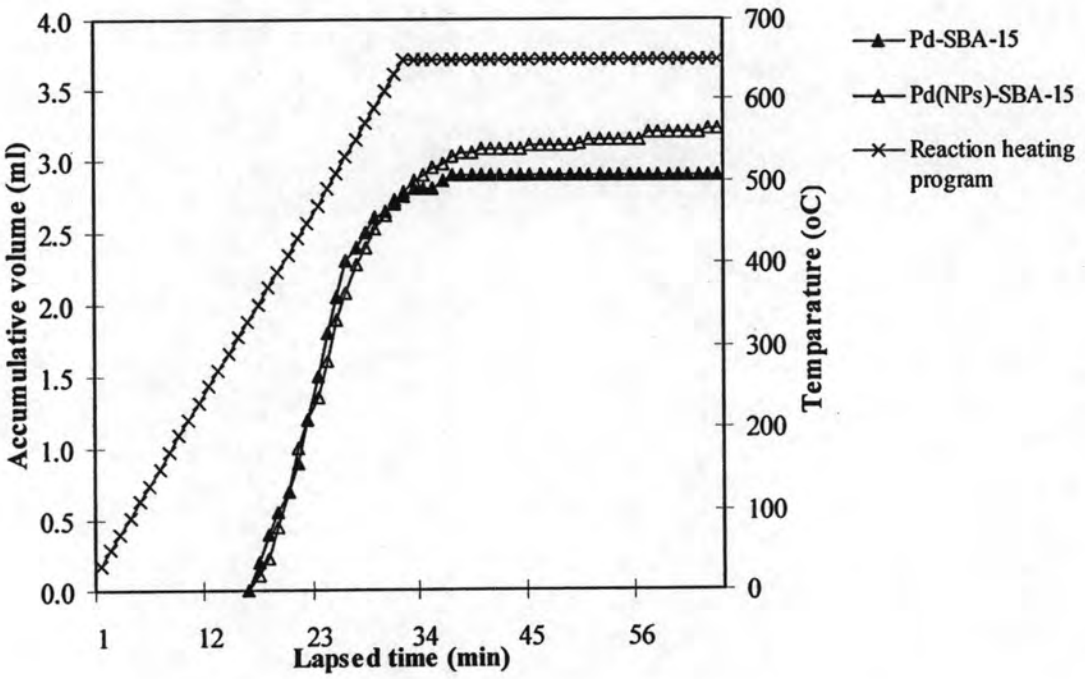

Figure 4.41 Accumulative volume of liquid fraction from Pd-SBA-15 cracking of glycerol waste at various particle size of Pd (Condition: N_2 flow of 20 ml/min, 650°C and reaction time of 40 min).

The conversion and product yield of glycerol waste cracking over Pd-SBA-15 and Pd(NPs)-SBA-15 were shown in Table 4.9. The conversion values were nearly equal, *i.e.* only 1.7% lower in case of Pd(NPs)-SBA-15. However, the yield of gas and liquid fractions were different about 8% and 6%, respectively. The smaller Pd particles promoted liquid product more than Pd-SBA-15. This could imply that active size was mainly Pd on the SBA-15 support.

Table 4.9 Value of %conversion and %yield obtained from Pd-SBA-15 cracking of glycerol waste at various particle size of Pd (Condition: N_2 flow of 20 ml/min, 650°C and reaction time of 40 min)

	Pd-SBA-15	**Pd(NPs)-SBA-15**
% Conversion[a]	86.80	85.10
% Yield[b]		
1.Gas fraction	33.20	25.40
2.Liquid fraction	53.60	59.70
- distillated liquid	18.29	22.73
- heavy liquid	35.31	36.97
3.Residue	13.20	14.90
Total volume of liquid fraction (ml)	3.00	3.30
Liquid fraction density (g/ml)	0.90	0.91

[a]*deriviation within 0.40%*
[b]*deriviation within 0.50%*

Figure 4.42 showed gas distribution obtained by catalytic cracking of glycerol waste over Pd-SBA-15 and Pd(NPs)-SBA-15 catalysts. Among gas products, formation of CO, CO_2, C5+, methane and 1,3-butadiene were favored. The composition of cracking product depends on particle size of metal on SBA-15. Figure 4.43 showed product distribution of distillated liquid, Pd-SBA-15 gave 2-cyclopenten-1-one as a main product while Pd(NPs)-SBA-15 promoted 2-propen-1-ol.

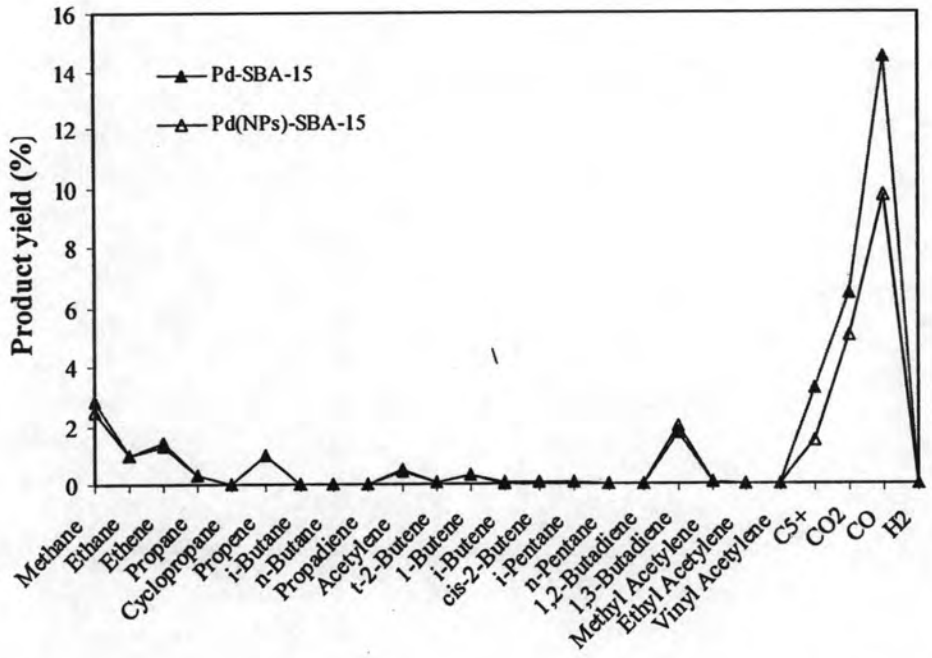

Figure 4.42 Distribution of gas fraction obtained from Pd-SBA-15 cracking of glycerol waste at various particle size of Pd (Condition: N_2 flow of 20 ml/min, 650°C and reaction time of 40 min).

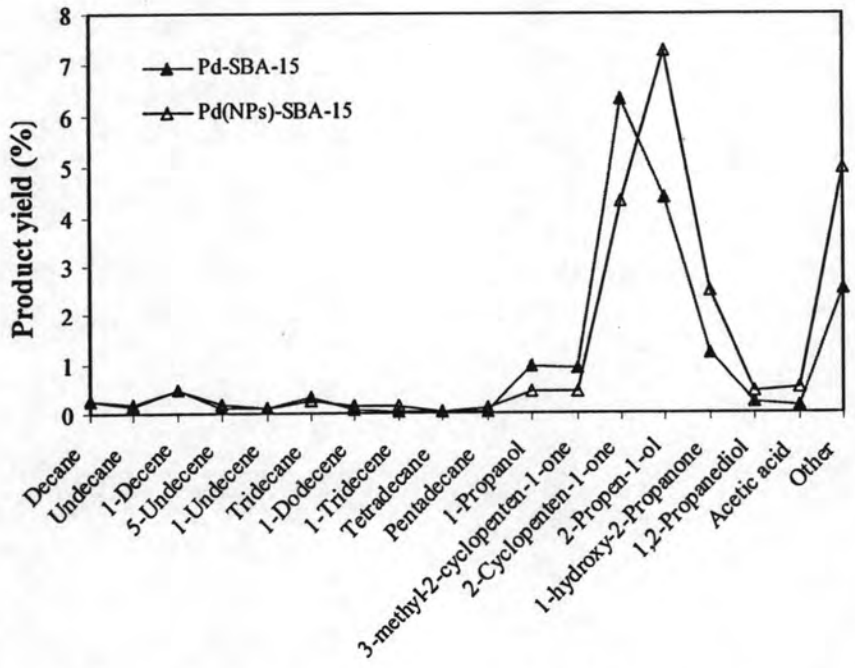

Figure 4.43 Distribution of liquid fraction obtained from Pd-SBA-15 cracking of glycerol waste at various particle size of Pd (Condition: N_2 flow of 20 ml/min, 650°C and reaction time of 40 min).

In catalytic cracking cases, the used catalysts were washed with n-hexane, dried and calcined. All catalysts cannot be regenerated because the catalyst was synthesized in acid condition but the glycerol waste was a base media (pH = 10.47) which the catalyst directly contacted to glycerol waste so it was able to destroy hexagonal framework of catalyst. The evidence of damaged hexagonal structure was confirmed by XRD pattern showed in Figure 4.44. In general, zeolite or mesoporous synthetic methods were necessary to dissolve the silica source with alkali solution at the pH around 10 to from SiO_2. In addition, the synthesized materials must be separated from the alkali media after finishing crystallization because it can be dissolved in base media and transform to other phases.

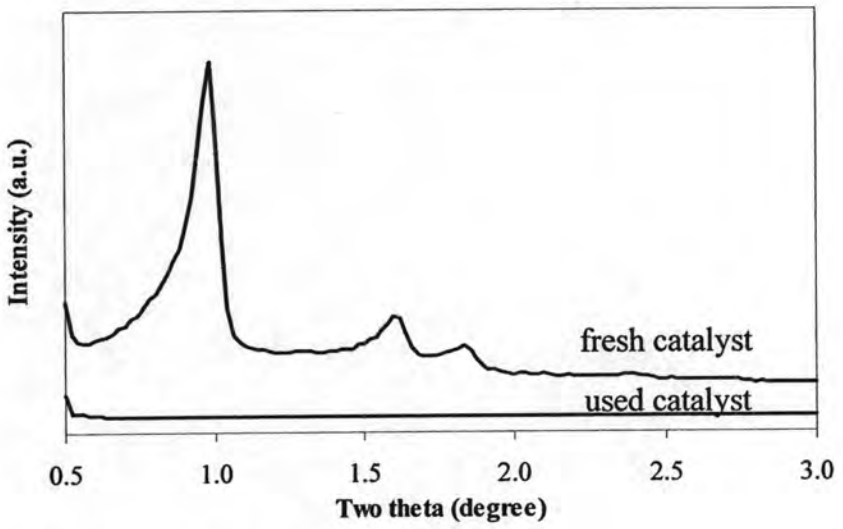

Figure 4.44 XRD patterns of the fresh and used catalysts.

4.7.4 Effect of position of catalyst

In order to solve a problem of recycling catalyst, the starting material should be placed in vapor phase. The experiments were set up at the reaction temperature 650°C, with 10 wt% of Pd-SBA-15 catalyst but two positions of the catalyst were test normally from liquid-phase (catalyst was mixed with starting material at the bottom of a 36 cm long reactor) catalytic cracking and new type vapor-phase (catalyst was placed on the 150 mesh sieve at 13 cm from the bottom of the reactor in order to contact vapor phase of starting material) catalytic cracking.

The kinetic rates two catalytic locations showed in Figure 4.45. At initial reaction time, liquid phase of starting material was obviously faster than starting material in vapor phase. That might be the effect of catalyst being in the phase of glycerol waste as starting material then it could overcome diffusion effect between starting material and catalytic active site. After 34 min, the reaction rates were no significant difference.

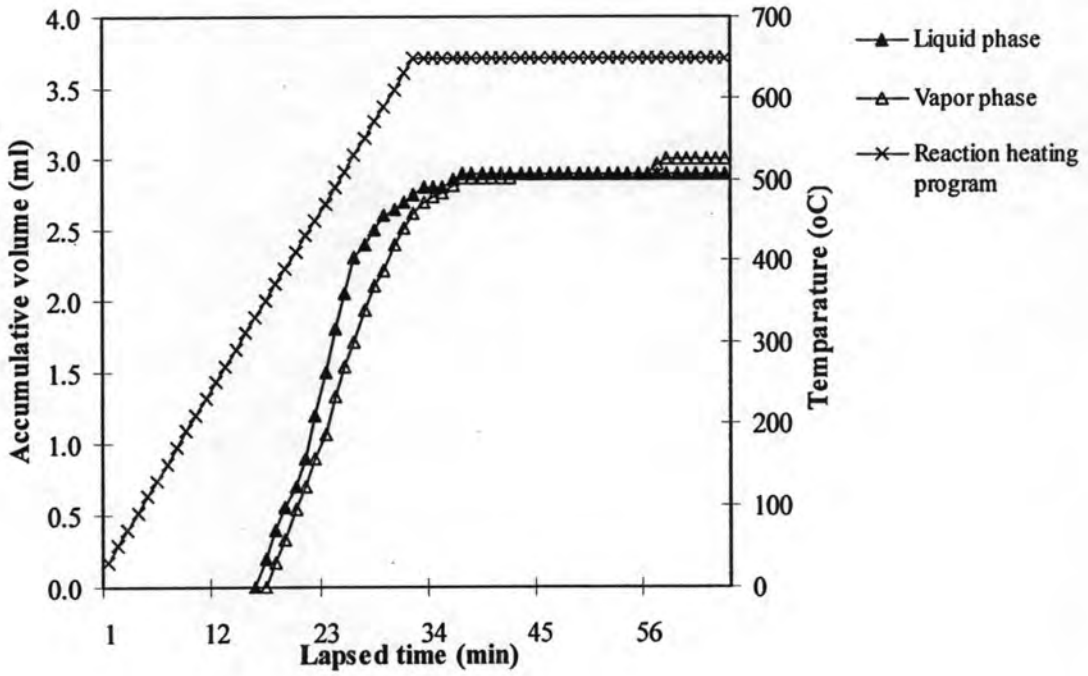

Figure 4.45 Accumulative volume of liquid fraction from Pd-SBA-15 cracking of glycerol waste at various position of catalyst (Condition: N_2 flow of 20 ml/min, 650°C and reaction time of 40 min).

The conversion value and product yield from two type of starting material phases were showed in Table 4.10. The conversion values of two cases performed reversely yield of gas fraction and liquid fraction. Particularly, in case of vapor phase gave gas fraction 5.8% lower than liquid phase and vapor phase gave liquid fraction higher than gas phase about 3.5%. Furthermore, the catalyst in vapor phase can recycle for the next batch.

Table 4.10 Value of %conversion and %yield obtained from Pd-SBA-15 cracking of glycerol waste at various position of catalyst (Condition: N_2 flow of 20 ml/min, 650°C and reaction time of 40 min)

	Liquid phase	**Vapor phase**
% Conversion[a]	86.80	84.47
% Yield[b]		
1.Gas fraction	33.20	27.40
2.Liquid fraction	53.60	57.07
- distillated liquid	18.29	24.17
- heavy liquid	35.31	32.90
3.Residue	13.20	15.53
Total volume of liquid fraction (ml)	3.00	3.10
Liquid fraction density (g/ml)	0.90	0.91

[a]*deriviation within 0.50%*
[b]*deriviation within 0.60%*

Gas and liquid products distributions of starting material phase study presented in Figure 4.46 and 4.47, respectively. The favored gaseous products were CO, CO_2, C5+, 1,3-butadiene and methane. The selectivity of gas fraction was similar in range hydrocarbon gas but different in quantity at permanent gas. In addition, the selectivity of distillated liquid component was different. Liquid phase starting material produced mainly 2-cyclopropen-1-one while vapor phase promoted 2-propen-1-ol. Catalytic liquid phase reaction produced high amount of syngas while vapor phase gave product distributions nearly same as thermal cracking.

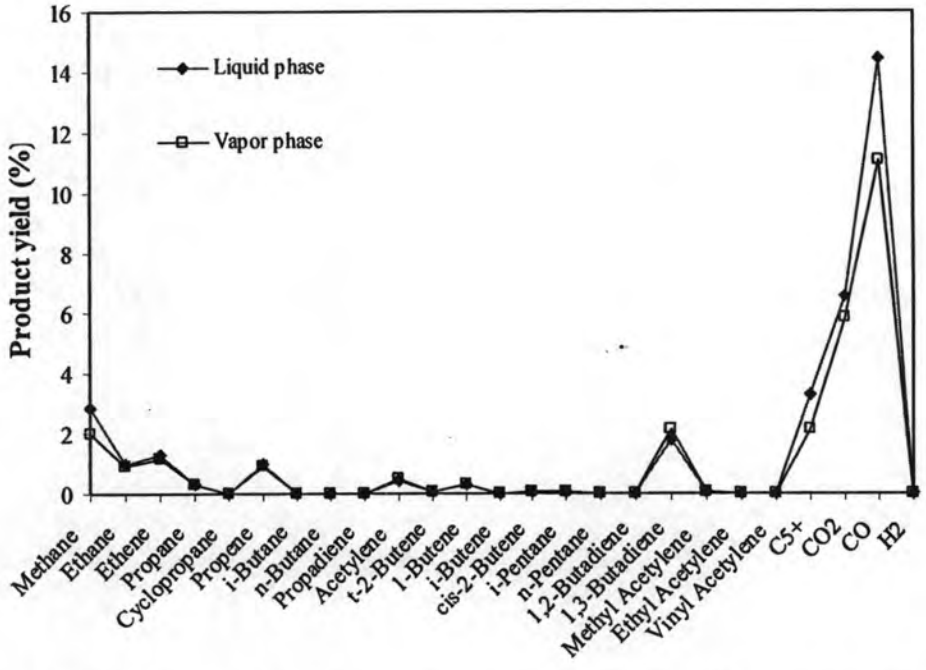

Figure 4.46 Distribution of gas fraction obtained from Pd-SBA-15 cracking of glycerol waste at various position of catalyst (Condition: N_2 flow of 20 ml/min, 650°C and reaction time of 40 min).

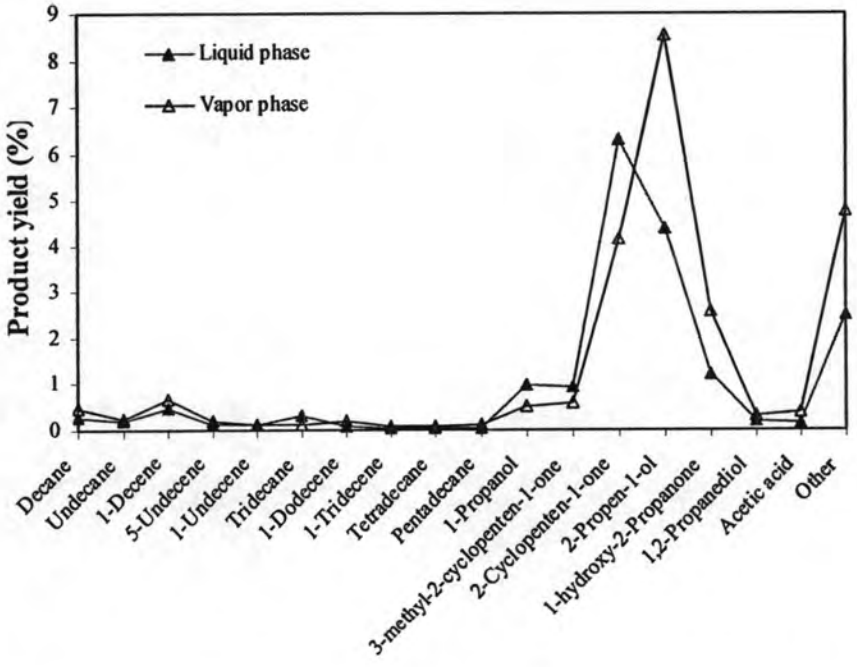

Figure 4.47 Distribution of liquid fraction obtained from Pd-SBA-15 cracking of glycerol waste at various position of catalyst (Condition: N_2 flow of 20 ml/min, 650°C and reaction time of 40 min).

4.8 Regeneration of catalyst

In case of starting material in vapor phase, catalyst can be recycled in the next reaction. The used Pd-SBA-15 catalyst of the first and the second runs were washed several times with n-hexane and dried in oven. The used catalysts were regenerated by calcination in air at 500°C for 4h and characterized by XRD technique, surface area analysis, SEM-EDS method before catalytic testing in the next reactions.

4.8.1 Characterization of regenerated catalyst

After calcination, regenerated catalysts were characterized by XRD technique and surface area analysis. Figure 4.48 showed the XRD patterns of fresh and regenerated catalysts, which confirmed for both first and second regenerated Pd-SBA-15 still remained three characteristic peaks of hexagonal phase like the fresh catalyst. During calcination, Pd metals were oxidized with oxygen to form large particle size of PdO [27]. Thus, the regenerated catalysts were shifted slightly too high angle than fresh catalyst. The adsorption-desorption isotherms of those catalysts presented in Figure 4.49. The regenerated catalyst showed the characteristic isotherm of mesoporous materials with the specific surface area of 290 m^3/g that was reduced about 61% as compared to the fresh catalyst (740 m^3/g) due to block coke formation in mesoporous pore. The amount of Pd on supported SBA-15 after calcination from SEM-DES method compared to fresh Pd-SBA-15 maintained Pd loading in range 2%.

Table 4.11 Textural properties of fresh and regenerated Pd-SBA-15 catalysts

	Fresh Pd-SBA-15	**1st regenerated Pd-SBA-15**	**2nd regenerated Pd-SBA-15**
Specific surface area[a] (m^3/g)	740	293	290
%Pd loading[b]	2.85	2.58	2.28

[a]Calculated using the BET plot method,
[b]Calculated using SEM-EDS method

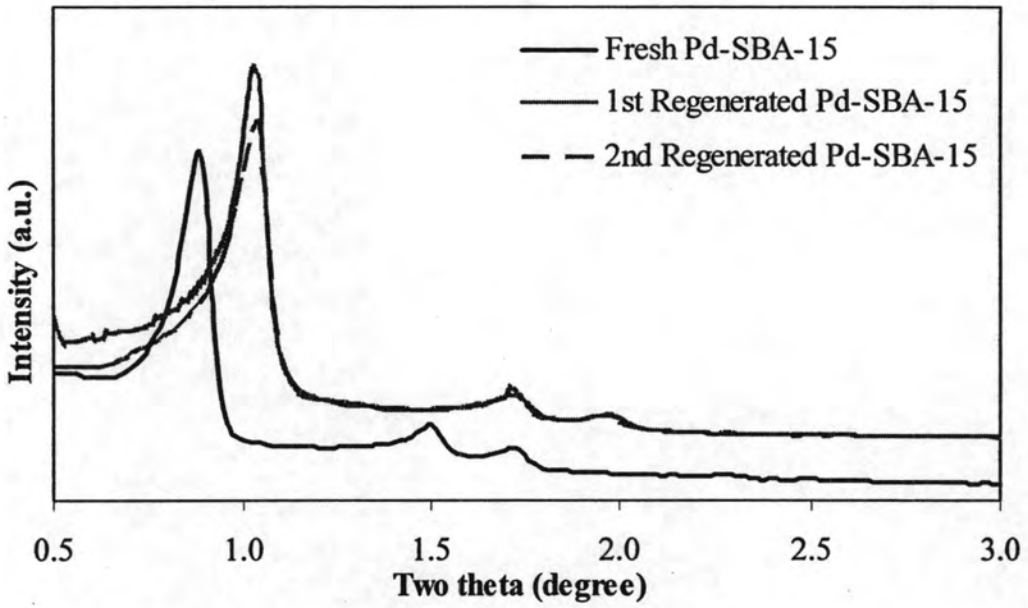

Figure 4.48 XRD patterns of fresh Pd-SBA-15, first regenerated Pd-SBA-15 and second regenerated Pd-SBA-15.

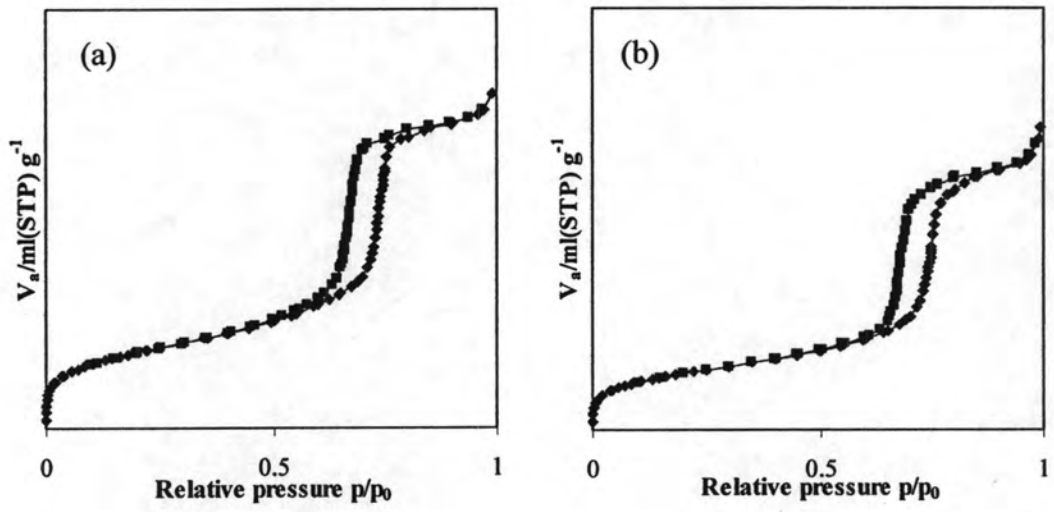

Figure 4.49 N_2 adsorption-desorption isotherm of (a) first regenerated Pd-SBA-15 and (b) second regenerated Pd-SBA-15.

4.8.2 Glycerol waste cracking over regenerated catalysts

The plots of accumulative liquid volume versus lapsed time of glycerol waste over fresh, first regenerated and second regenerated Pd-SBA-15 catalysts showed in Figure 4.50. At the beginning there were no significant difference reaction rates. After 26 minute, regenerated catalysts produced liquid fraction slower than fresh catalyst. Therefore, the total liquid volumes of these three catalysts were reduced by a number of uses due to the effect of surface area of catalysts or amount of Pd in catalyst.

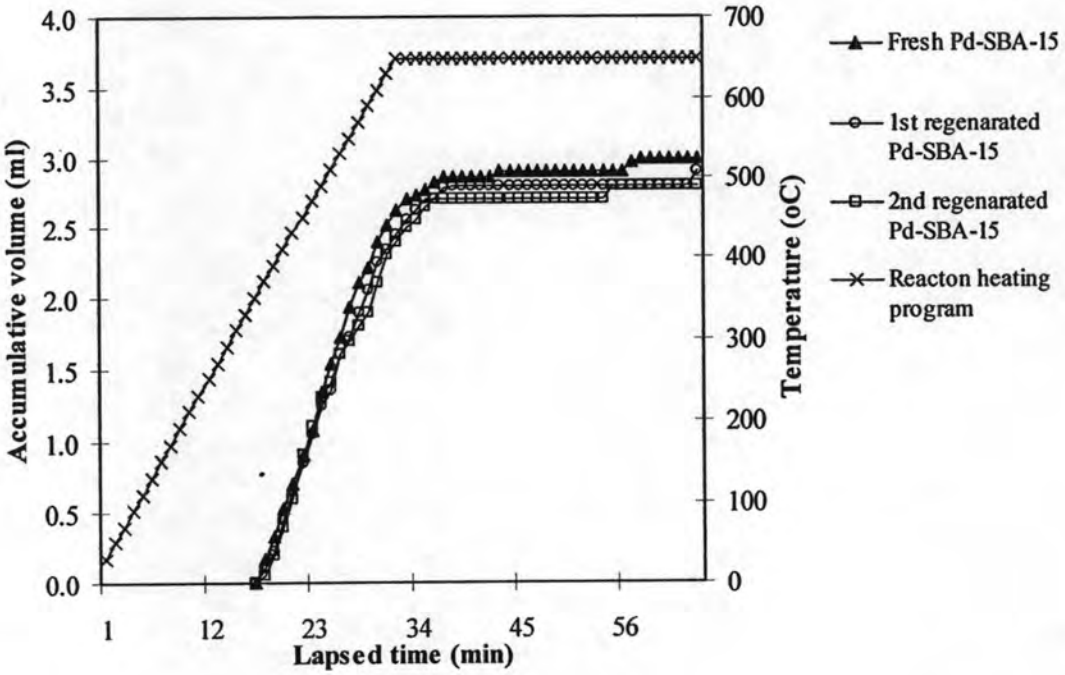

Figure 4.50 Accumulative volume of liquid fraction from catalytic cracking of glycerol waste over fresh, first regenerated and second regenerated Pd-SBA-15 catalyst (Condition: N_2 flow of 20 ml/min, 650°C and reaction time of 40 min).

The conversion and product yield from glycerol waste cracking over fresh, first regenerated and second regenerated Pd-SBA-15 catalysts were shown in Table 4.12. The conversion value about 82% obtained from regenerated catalysts which was 2.2% less than fresh catalyst. As compared to the fresh catalyst, the yields of gas fraction obtained from regenerated catalysts were relatively high.

Table 4.12 Value of %conversion and %yield obtained from catalytic cracking of glycerol waste over fresh, first regenerated and second regenerated Pd-SBA-15 catalyst (Condition: N_2 flow of 20 ml/min, 650°C and reaction time of 40 min)

	Fresh Pd-SBA-15	**1st regenerated Pd-SBA-15**	**2nd regenerated Pd-SBA-15**
% Conversion[a]	84.47	82.20	82.20
% Yield[b]			
1.Gas fraction	27.40	28.60	30.80
2.Liquid fraction	57.07	53.60	51.40
- distillated liquid	24.17	22.89	21.91
- heavy liquid	32.90	30.71	29.49
3.Residue	15.53	17.80	17.80
- wax	14.38	16.54	16.72
- solid coke	1.15	1.26	1.08
Total volume of liquid fraction (ml)	3.10	3.05	2.90
Liquid fraction density (g/ml)	0.91	0.88	0.89

[a]*deriviation within 0.50%*
[b]*deriviation within 0.60%*

Gas and liquid products distributions in regenerated catalyst study were presented in Figure 4.51 and 4.52, respectively. These results were nearly similar to each others with major gaseous product as CO, CO_2, 1,3-butadiene, C5+ and methane. The liquid product distributions for the fresh and regenerated catalysts were still 2-cyclopropen-1-one and 2-propen-1-ol. As a result, it could be concluded that the used catalyst was stable and could be regenerated. The cracking activity of regenerated catalyst performed no significant difference in second and third runs when compared to the first run of the fresh catalyst.

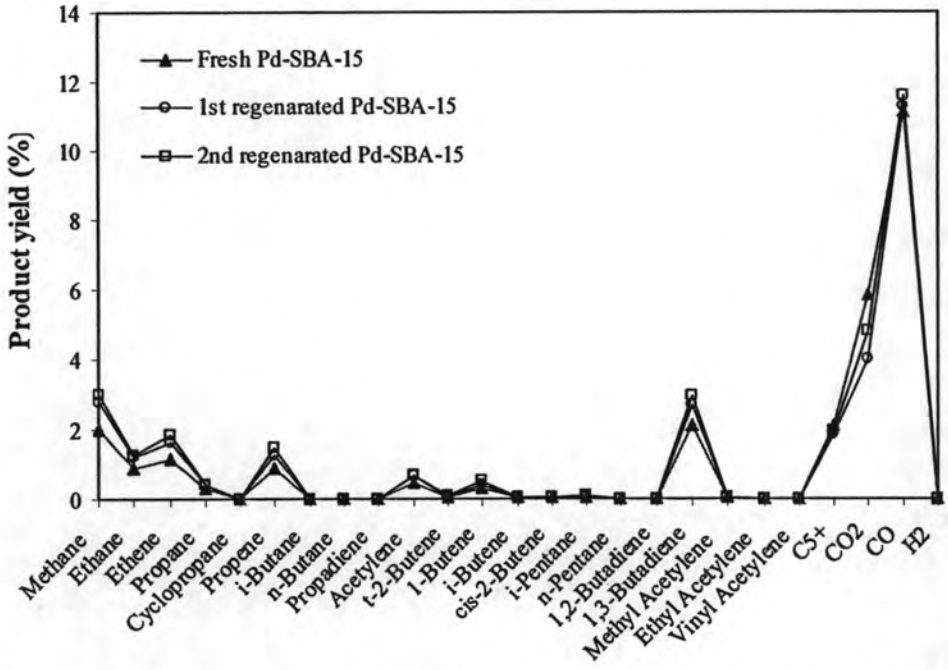

Figure 4.51 Distribution of gas fraction obtained from catalytic cracking of glycerol waste over fresh, first regenerated and second regenerated Pd-SBA-15 catalyst (Condition: N_2 flow of 20 ml/min, 650°C and reaction time of 40 min).

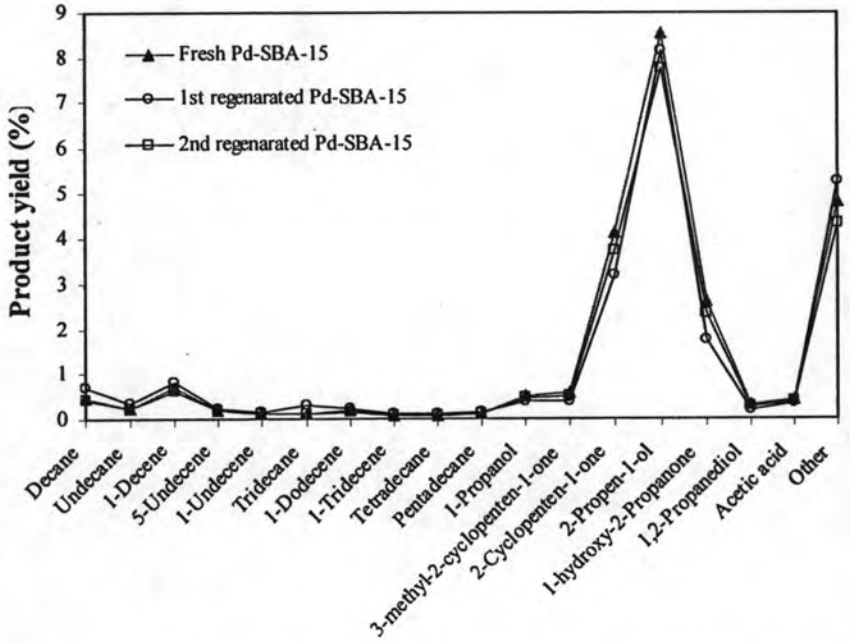

Figure 4.52 Distribution of liquid fraction obtained from catalytic cracking of glycerol waste over fresh, first regenerated and second regenerated Pd-SBA-15 catalyst (Condition: N_2 flow of 20 ml/min, 650°C and reaction time of 40 min).